UNITED NATIONS UNIVERSITY
UNU-GTP
Geothermal Training Programme

Orkustofnun, Grensasvegur 9,
IS-108 Reykjavik, Iceland

Reports 2016
Number 26

BOREHOLE GEOLOGY, HYDROTHERMAL ALTERATION AND STRUCTURE OF WELL SV-26 IN THE SVARTSENGI AREA, SW-ICELAND

Andrei Eugen Lup
SC Daflog SRL
Mediaș, str. Nicolae Titulescu nr. 3
ROMANIA

ABSTRACT

This report describes the stratigraphic sequence and alteration in drill hole SV- 26 in the Svartsengi high-temperature field, SW-Iceland. Well SV-26 is a make-up and exploration well for the Svartsengi power plant. It is a directional well deviated to the east towards the southern part of Mt. Sýlingarfell to explore and extend the southeastern part of the Svartsengi production field. The stratigraphy of well SV-26 is characterized by basaltic lava flows and different hyaloclastite formations. Drill cuttings in the uppermost part of the well are characterized by a high degree of oxidation. Three alteration zones were observed: Unaltered zone (0-112 m), smectite-zeolite zone (112-622 m) and chlorite-epidote zone (622-1394 m). No drill cuttings were available for analysis below 1394 m due to total loss of circulation within the well. Aquifers in this well were located based on borehole measurements and records of circulation losses. It is important to note that the temperature loggings and mineral sequences of SV-26 do not show any evidence of temperature reversal which implies that the Svartsengi geothermal system could extend further to the east than previously believed.

1. INTRODUCTION

1.1 Geology of Iceland

Geographically, Iceland is in the northern part of the Mid-Atlantic Ridge between Greenland and Norway at 63 °23‟N to 66 °30‟N. Iceland has an area of 103,106 km^2 and an average altitude of 500 m making it the third largest island located in the Atlantic Ocean (Jakobsson, 1979; Saemundsson, 1979). The subaerial part represents about 30% the Iceland Basalt Plateau, which rises more than 3,000 m above the surrounding sea floor and covers about 350,000 km^2 (Thórdarson, 2012). Geologically, Iceland is a very young land mass that started to form in Early Miocene, about 25 million years ago but the oldest rocks that can be found exposed on the surface belong to the Tertiary period around 16 million years ago (Hardarson et al., 1997). The construction of Iceland is a consequence of a stationary plume and the spreading of two tectonic plates: American and Eurasian, which move apart at an average rate of 1 cm per year in each direction. This spreading started about 70 million years ago and the plate boundary is delineated by series of faults and volcanoes, which together form a distinguishing ridge-like structure in the middle of the ocean. Iceland resides on a mantle plume, which has been active for

the last 65 million years and has caused significant volcanic activity. These eruptions are effusions of basaltic lava from fissures or shield volcanoes. Volcanism, sedimentation and erosion are more active in Iceland than in other places, changing the surface radically in a relatively short time. Iceland is the only place where the active spreading and plate growth of the Mid-Atlantic Ridge can be seen because this is the only section of the plate boundary exposed above the sea level. The narrow belts of active faulting and volcanism spreading from Reykjanes in the southwest, which zig-zag across Iceland all the way to the north and into the Arctic Ocean, represent the surface expressions of this plate boundary (Thórdarson, 2012).

The three main geological formations in Iceland are shown in Figure 1. The oldest are successions of lava that generally dip gently towards the volcanic zones and belong to the Tertiary formation (3- 16 my). The second formation is of Quaternary, Plio-Pleistocene age (0.7-3 m.y.). The succession is comprised of alternating sequences of lavas and hyaloclastites. The lavas were formed during interglacial periods while the hyaloclastites were created as a result of subglacial eruptions during ice ages. The third and youngest formation is contained within the neovolcanic zone and is composed of Upper-Pleistocene and Postglacial formations (< 0.7 m.y.) (Saemundsson, 1979; Rodas, 1996).

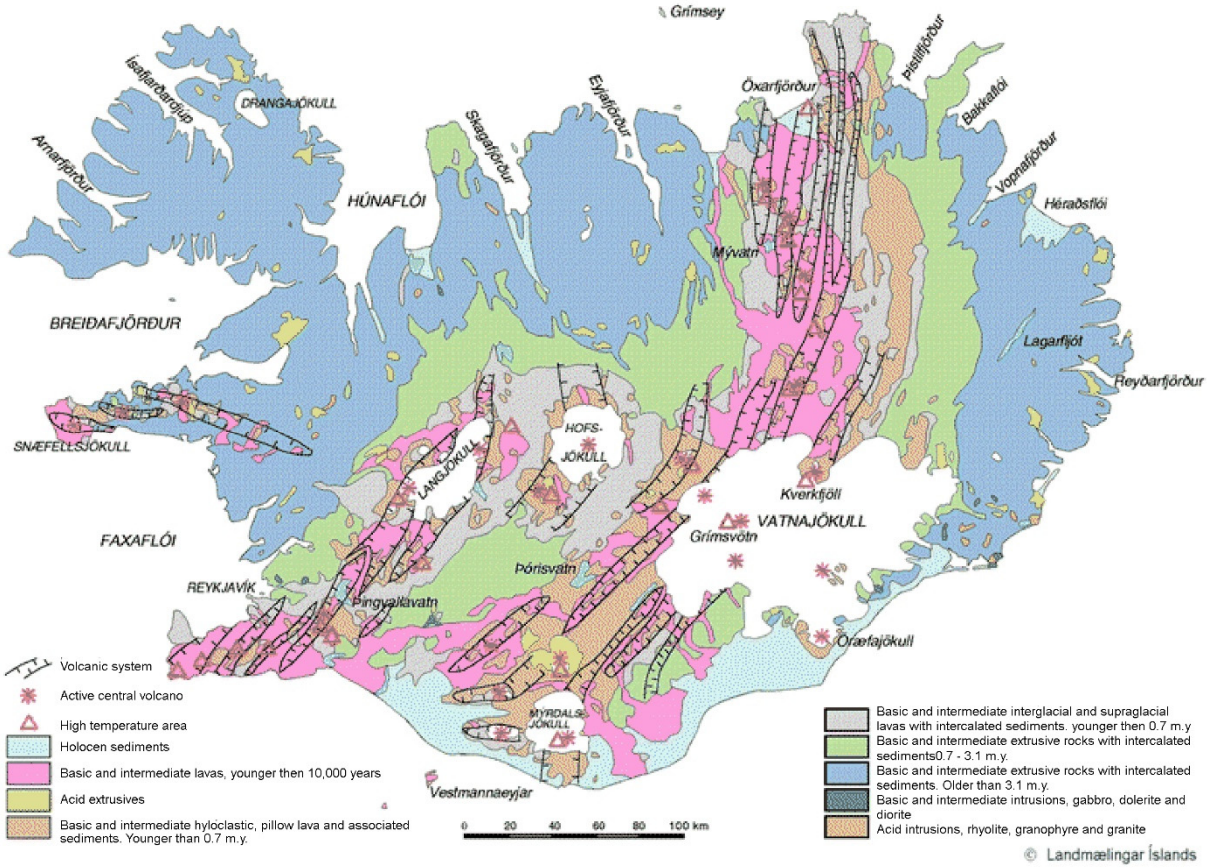

FIGURE 1: Geological map of Iceland showing oldest Tertiary rocks, older Plio-Pleistocene eruptives, Holocene rocks plus other young formations; volcanic systems follow the oceanic ridge (based on Jóhannesson and Saemundsson, 1999)

Due to intense volcanism and very active tectonics, Iceland is rich in geothermal resources. The geothermal areas in Iceland are classified as high or low in temperature, based on the geological setting and temperature information collected from loggings in the areas. Most of the high-temperature areas are within the active volcanic belts, but most of the low-temperature areas occur in Quaternary and Tertiary formations.

In the high-temperature areas, the underground temperature reaches 200°C within 1,000 m depth and the heat source is generally shallow magma intrusions (Björnsson et al., 2010). These areas are confined to the active volcanic zones (Figure 2). The surface manifestations are mostly steam vents because the topography and the high bedrock permeability of these very young rocks results in a deeper groundwater table.

Most of the low-temperature areas can be found flanking the active zone, and the largest of these can be found in southwest of the country. There are about 250 low-temperature areas, which do not exceed 150°C in the uppermost 1,000 m (Figure 2). The common surface manifestations are hot or boiling springs and to date, and over 600 hot springs (temperature over 20°C) have been located (Worku, 2012).

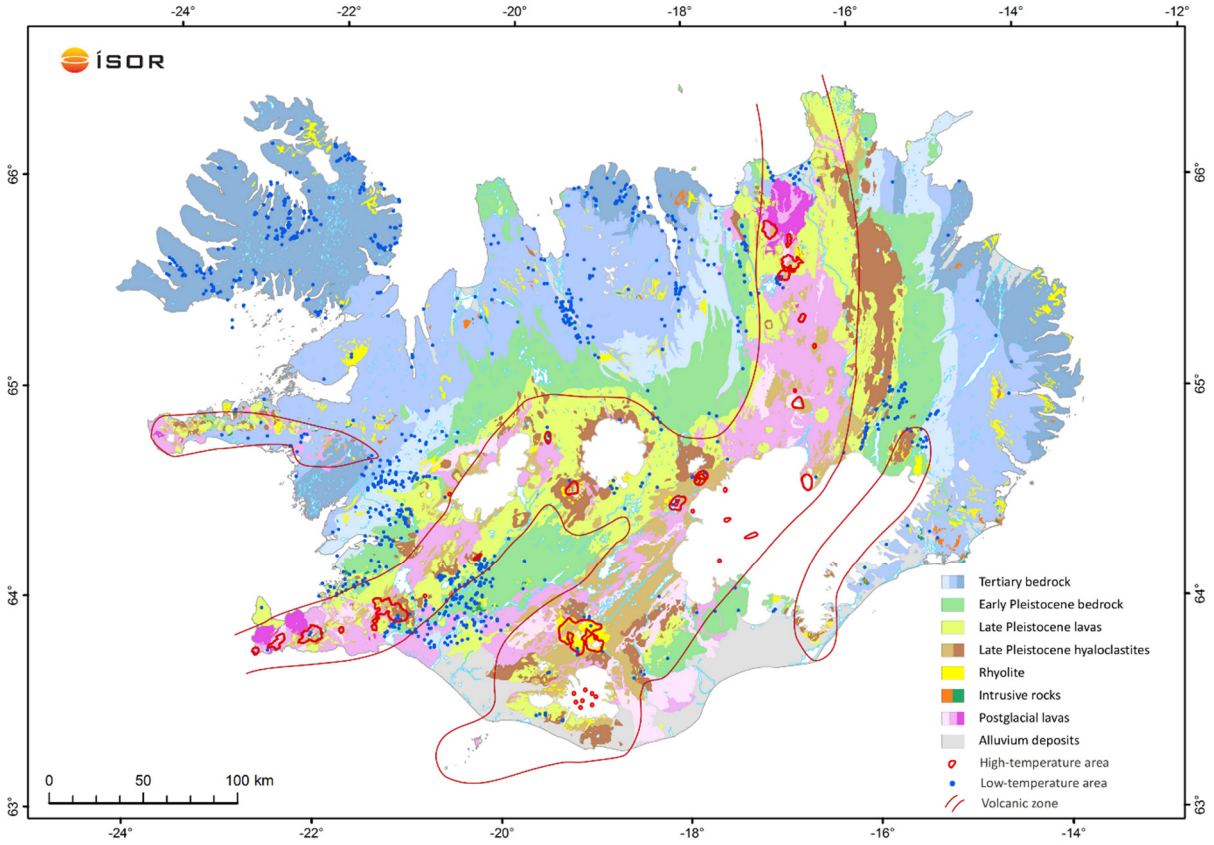

FIGURE 2: Geological map of Iceland showing high-temperature and low-temperature areas (Hjartarson and Saemundsson, 2014)

1.2 Local geology

In southwest of Iceland, the geology spans over the last 3.2 million years, since the very last stages of the Pliocene across the Quaternary to the present day. Outcrops of the oldest rocks can be found in and around Mt. Esja (Figure 3) in the north, and the succession gradually becomes younger towards the south. The submarine Reykjanes Ridge and the West Volcanic Zone are connected by the axis of the Reykjanes Volcanic Belt along which the youngest rocks outcrop (Figure 3). From east to west, the belt comprises four volcanic systems: the Hengill, Brennisteinsfjöll, Tröllladyngja, and Reykjanes systems. The systems have a north-easterly strike and extend across the peninsula (Thórdarson, 2012).

The Svartsengi area is located on the Reykjanes Peninsula, approximately 50 km southwest of the capital Reykjavik, and covers the Svartsengi geothermal field, the lava fields surrounding it, and the pillow lava piles of Hagafell, Lagafell and Thorbjarnarfell and the table mountain of Svartsengisfell. An active

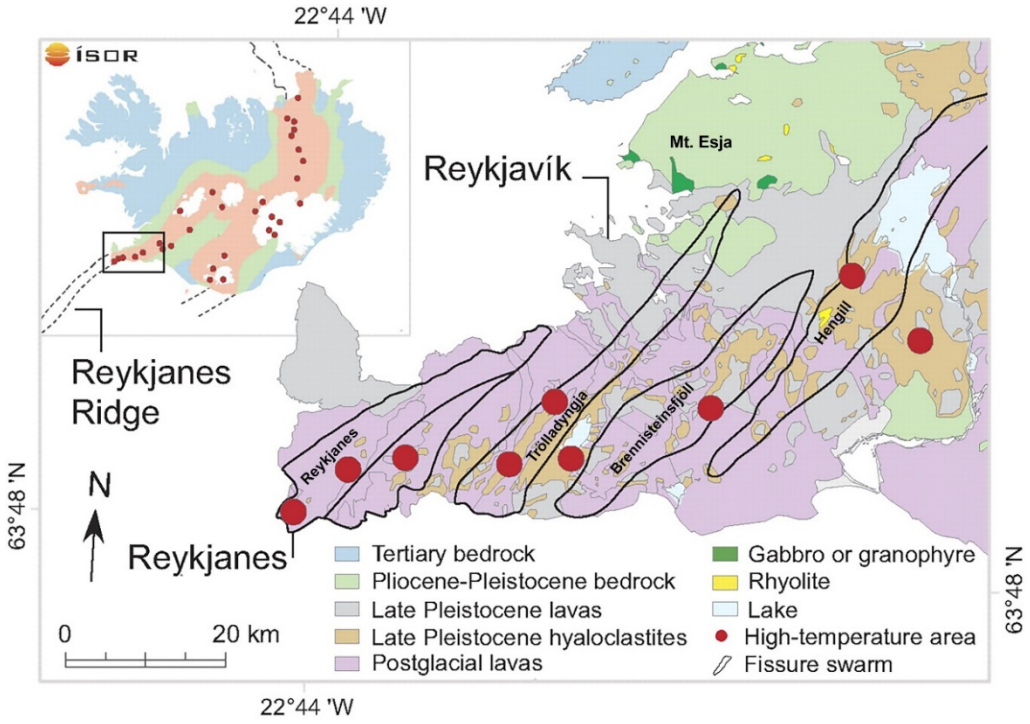

FIGURE 3: The main geological features of the Reykjanes Peninsula

fissure swarm cutting across the field causes the geothermal field to have a very high degree of faulting, but surface manifestations are scarce and surface alteration is relatively small (Rodas, 1996).

Fissure swarms are described in the geological literature of Iceland as being part of a volcanic system with anomalous volcanic accumulation rates, especially in its central part. The elevation of the lava plain at Svartsengi only rises about 30 m above sea level, and there is no indication of an anomalous volcanic production linked with the central part of the fissure swarm which could denote a central "volcano activity". A central underlying heat source, in the form of a magma chamber, for the geothermal system may therefore be unlikely (Franzson, 2017).

The Svartsengi high-temperature field lies within the Grindavík fissure swarm, which is the second west most fissure swarm on the Reykjanes Peninsula (Figure 3). About 30 eruptions are believed to have occurred within the swarm during Holocene age (Postglacial) and are mostly fissure eruptions (Jakobsson et al., 1978). The oldest rock formations outcrop at Mt. Thorbjörn and Svartsengisfell mountains, consist, to a large extent, of pillow lavas and some hyaloclastites. The second main geological surface formation comprises both aa and pahoehoe lava types. These lavas are postglacial flows (< 12 ka) and cover the entire high-temperature area. At the northern foot of Mt. Thorbjörn there are two small lava craters. The lavas released from the two small craters that can be found at the northern foot of Mt. Thorbjörn are likely to be found underlying the topmost lava to the north and east. The Svartsengi area is mainly covered by the two youngest lavas, the northern one originated from an approximately 10 km long fissure to the east of Svartsengisfell, and the lava flow to the south derived from a short fissure west of Mt. Thorbjörn. These lavas are mostly of aa type (Rodas, 1996).

1.3 Tectonic setting

The main tectonic faults and fissures shown in Figure 4 are dominantly NE-SW aligned and are a part of the Reykjanes-Svartsengi NE-SW fissure swarm. A few N-S structural features are shown mainly in Svartsengisfell and to the south from there. As expected in an area of continuous seismic activity, the tectonic structures are more pronounced in the oldest formations but sporadic in the most recent formations. The most noticeable faults are those forming the ca. 200 m wide graben in Mt Thorbjörn.

The throw of these faults, however, are most pronounced in the centre of the mountain but decreases rapidly in both directions, indicating a topographic effect on the dimension of the throw (Franzson, 2017).

In order to clarify further faults, fractures and geothermal manifestations in and around Svartsengi, a separate tectonic study was made, mainly based on aerial photographs (Franzson, 1990). As previously mentioned, the tectonic and volcanic features are most noticeable in the older formations, while largely absent in the youngest lavas. The main tectonic lineation in Thorbjörn hyaloclastite formation is NE-SW and a relatively strong northerly trend is observed in Selháls, south of Svartsengi. These have been confirmed by a ground study where the northerly fracture directions are obvious in the southern part of the Svartsengisfell hyaloclastite formation. This fracture trend extends towards the Svartsengi well field in the north and probably carpeted there by the young Illahraun fissure lava (Franzson, 2017).

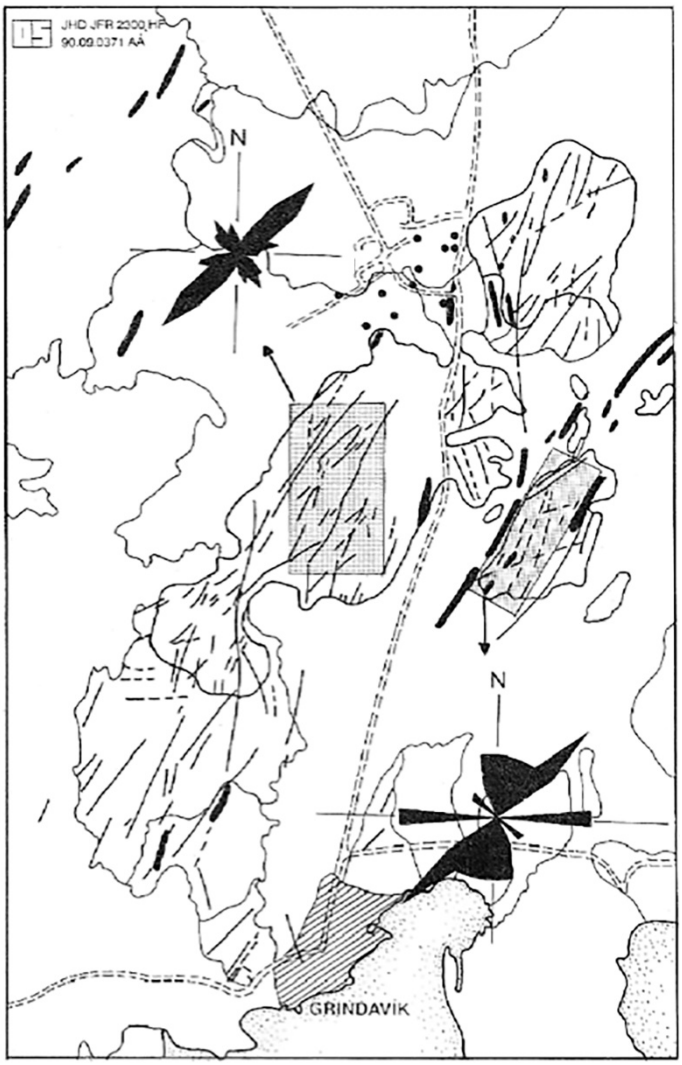

FIGURE 4: Tectonic lineaments around Svartsengi along with rose diagrams of fracture orientation deduced from ground study (Franzson, 1990; 1995)

1.4 Previous studies at the Svartsengi area

Previous work done in the area consists of geological mapping by Kuthan (1943), Jónsson (1978), Sigurdsson (1985) and Jóhannesson (1989). Hjalti Franzson (1990) mapped the surface alteration and structural lineation of the geothermal field. According to the degree of surface alteration intensity, three alteration zones have been defined: high, medium and low. High-intensity alteration is found where widespread formations of clay occur; medium intensity alteration is characterized by extensive deposition of silica, in the form of opal crusts, and/or aragonite, and low-intensity alteration is characteristic of slight deposition of silica, also in the form of opal crusts. Active manifestations are depicted by hot soil and steaming ground (Franzson, 1990; Rodas, 1996).

The area from Svartsengi to the Reykjanes high-temperature field has been investigated using resistivity surveys, ranging from the original dipole, Schlumberger, TEM, MT and an integrated TEM-MT survey, which can detect anomalies to more than 10 km depth. Figure 5 shows the 4 Ohm low resistivity anomalies at 200, 400 and 600 m depths within the Svartsengi drill field, which indicate the top of the geothermal system from an early TEM survey (Georgsson, 1984). The resistivity structures show an overall NE-SW alignment around the Svartsengi field, however there is a clear structural trend that is slightly west of north within the central of the field, and which appears to extend towards Selháls in the south. No apparent anomaly is observed around the steam cap in the north or below the hydrothermal alteration at the northern end of Svartsengisfell, which may indicate that that area there is at the outer periphery of the reservoir (Franzson, 2017).

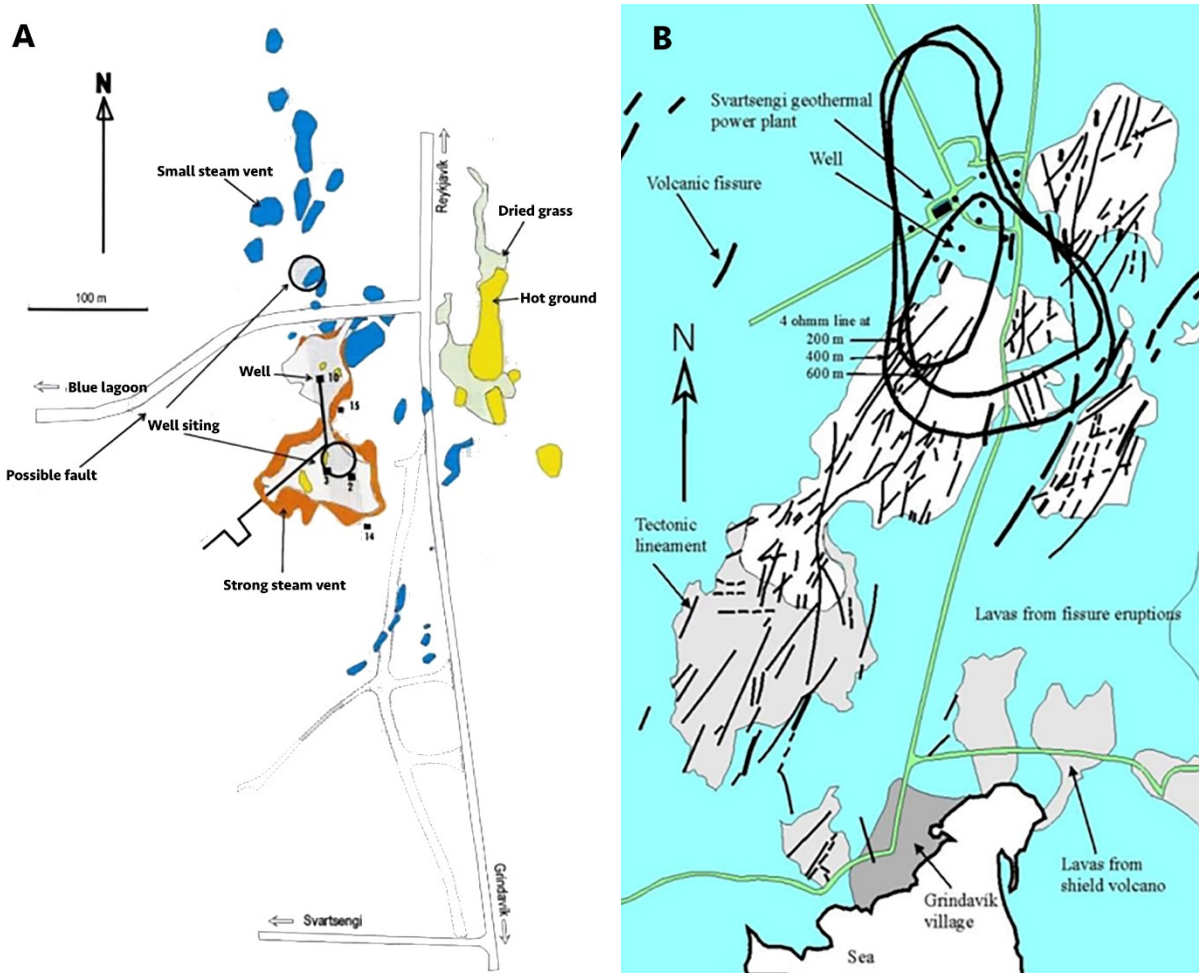

FIGURE 5: A) A sketch showing the surface features of the steam zone and the probable underlying tectonic lineaments that control the steam flow. B) Simplified geological map, tectonic lineaments and the shape of the shallow resistivity anomalies (Georgsson, 1984)

2. BOREHOLE GEOLOGY

2.1 Drilling well SV-26

Well SV-26 is a make-up and exploration well for the Svartsengi power plant (Figure 6). It was drilled from the same platform as SV-18. The well is located southeast of the power plant in Svartsengi. The planned depth of SV-26 was 2500 m or more. The final depth, however, was 2537 m. The location of well SV-26 and the well path is shown in Figure 6. Well head coordinates are: X = 331589.767 Y = 379078.146 Z = 24.6 m a.s.l. Drilling was planned towards the east to explore if the geothermal resource had an eastward extension. The aim was to drill a directional well through known faults within the southern part of Mt. Sýlingarfell in order to penetrate feed points to obtain maximum productivity in the well.

The planned design of well SV-26 and the division of the drilling into sections was as follows (Sigurdsson and Fridleifsson, 2015):

- Phase 0: Pre-drilling for surface casing with 26" bit to 100 m, cased with 22½".
- Phase 1: Drilling for anchor casing with 21" bit to 340 m, cased with 18⅝".

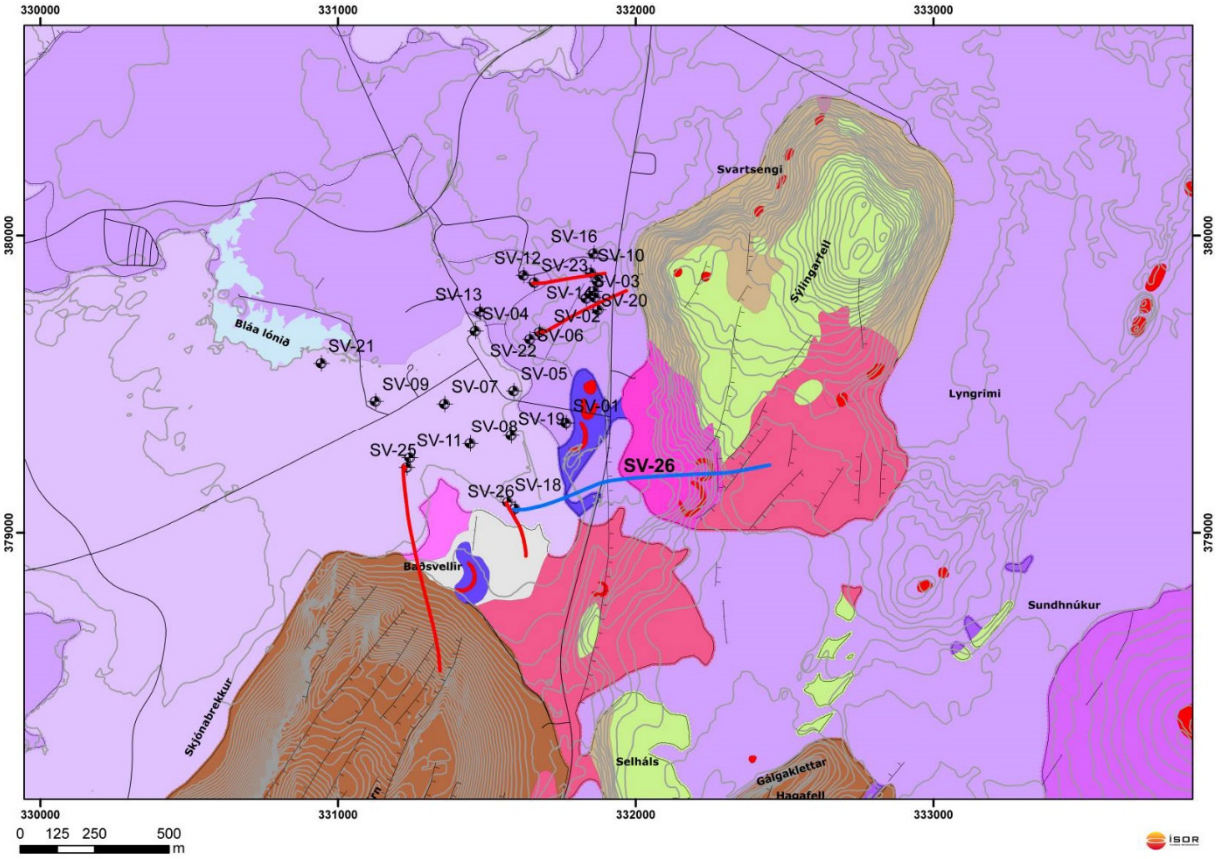

FIGURE 6: Geological map of the Svartsengi field (Saemundsson, 2015). It shows the trajectory path (solid blue line) of well SV-26

- Phase 2: Drilling for production casing with 17½" bit to 1000 m, cased with 13⅜".
- Phase 3: Drilling of the production part with 12¼" bit to about 2500 m, cased with 9⅝" perforated liner (Weisenberger et al., 2016).

The actual well as drilled deviates from the planned well design by an additional hanging casing as seen in Table 1. The well was drilled in 5 phases (0–4). An overview of the drilling phases and details of the casing depths are shown in Table 1. Figure 7 shows the drilling progress of well SV-26.

TABLE 1: Drilling and casing depths in well SV-26. All drilling and casing depths are measured from the rig floor (RF) of the Thor rig, 9.0 m above the ground level, except for the pre-drilling phase where depths are measured from the rig floor of Saga, 2.0 m above ground level

Drill-rig	Phase	Depth (m)	Depth reference	Bit Size	Casing type	Casing depth (m)	Casing depth reference
Saga	Pre-drilling	100.6	Saga RF	26"	22½"	99.8 m	Saga-RF
Thor	1. phase	352	Thor RF	21"	18⅝"	351	RF
Thor	2. phase	886	Thor RF	17½"	13⅜"	873.5	RF
Thor	3. phase	1250	Thor RF	12¼"	9⅝"	805.8-1247.5	RF
Thor	4. phase	2536.6	Thor RF	8"	7" (liner)	1203-2532.2	RF

Drill rig Saga was ready for drilling of the pre-drilling (phase 0) on the 4th of July, 2015. Drilling with a 26" air hammer into formation commenced the same morning. The drilling went slowly due to collapses in the well, causing seven cement jobs during drilling. Drilling, casing, and cementing of phase 0 were completed on July 15th and the drill rig Saga was ready for transportation, after a total of

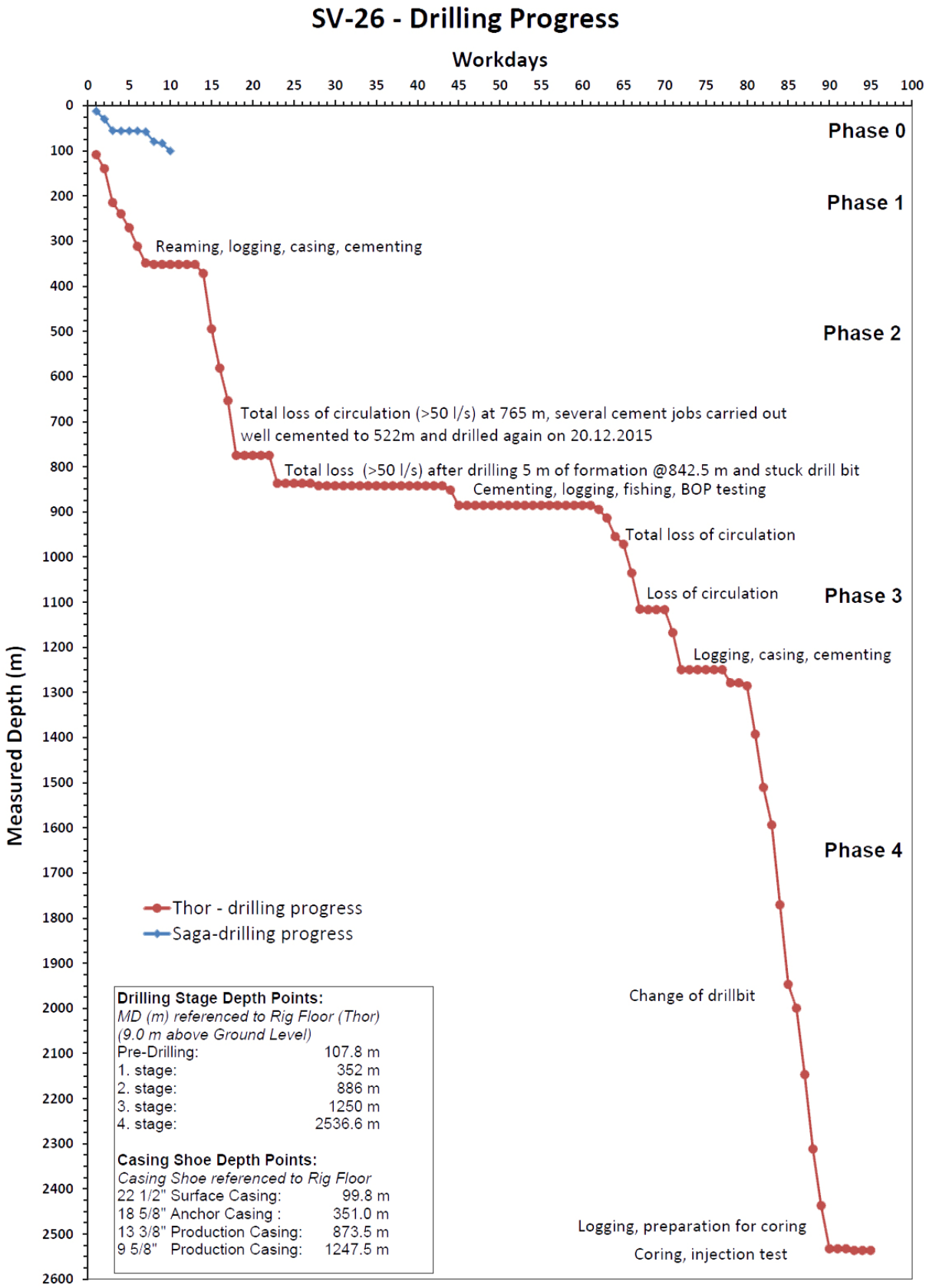

FIGURE 7: Drilling progress of well SV-26. Workdays of rigs Thor (red line) and Saga (blue line)

12 working days. At this point the well was 100.6 m deep from the rig floor of Saga, which corresponds to 107.8 m depth from the rig floor of Thor.

Preparation for the drilling of phase 1 with the drill-rig Thor started on November 29th with testing of the blow-out preventers. Drilling into a formation started the next day at 108 m. Phase 1 was finished on December 11th (workday 13 of Thor). An 18⅝" anchor casing was run down to 351 m depth with reference to the rig floor.

Drilling of phase 2 started on December 12th (workday 14), with testing of the blow-out preventers, and finished on January 16th (workday 49). Complications occurred during drilling of phase 2 due to repeated circulation losses in the well, resulting in 13 cement jobs. At a depth of 842.5 m the drill string got stuck on December 26th. It took 11 days to release the drill string, which occurred on January 5th. The well was drilled down to 886 m using rotary mud drilling method with a 17½" tri-cone drill bit and a 13⅜" production casing was run down to 873.5 m MD with reference to the rig floor of Thor. Cementing of the production casing was successful with total of 95.3 m^3 cement slurry used.

Rig operations of phase 3 started on January 17th 2016 (workday 50). After the installation and testing of the blow-out preventers the drilling crew was ready to run in the bottom hole assembly (BHA) with a 12¼ drill bit, motor and MWD. In the early morning on the 18th of January the elevator sprang open and parts of the BHA were lost in hole. The fishing procedures lasted for 8 days (January 18th to January 26th). Drilling into formation commenced on January 29th and was delayed by 2 total losses of circulations but drilling of phase 3 was completed on February 15th (workday 79) at a depth of 1250 m. A 9⅝" hanging casing was installed from 805.8 to 1247.5 m.

Rig operations on phase 4 started on February 16th 2016 (workday 80), with setting up and testing of the blow-out preventers. Drilling of phase 4 was finished on March 2nd (workday 95). The well was drilled down to a measured depth of 2534 m (with reference to the rig floor) using an 8½" drill bit. A total loss of circulation occurred at 1346 m and no cuttings were retrieved after 1394 m.

An attempt was made to drill a core on February 29th. However, coring had to be stopped after 3 meters of drilling at a depth of 2537 m, which is the final depth of the well but no core was retrieved from the core barrel. After the coring attempt, a liner was lowered into the well with the top of the liner being at 1203 m and bottom at 2532 m depth as measured from the rig floor.

2.2 Analytical methods

Binocular microscope
Rock cuttings at well SV-26 were sampled at an interval of 2 m. An Olympus binocular microscope was used to identify lithology, analyse grain size, oxidation, alteration minerals, veins, vein fillings and primary minerals. The analysis in the binocular microscope was done on wet samples to have clear visibility of any obscured features in the cuttings and acid was used to identify carbonates. An initial binocular microscope analysis was carried out at the drill-site but further detailed analyses were carried out at the ÍSOR labs in Reykjavik.

Petrographic microscope
The petrographic analyses are more accurate in determining the mineral assemblage of each stratigraphic unit and alteration mineralogy and was based on 11 thin sections selected from different depths. These were used to confirm rock type, texture, porosity, alteration minerals, alteration sequences and to identify additional minerals not seen in the binocular microscope. The petrographic analyses were also very helpful in identifying the alteration of primary minerals.

XRD analysis
The XRD analysis is a technique used to study crystallized materials based on the scattering of X-rays according to the crystal type of the material. The X-ray diffractometer analyses were carried out to

differentiate between various clay minerals. Each clay mineral group is characterized by a particular type of layer structure and interlayer material. Samples from SV-26 were collected and XRD analysed at ÍSOR XRD lab. The equipment used is a Bruker AXS D8 Focus, producing Cu kα radiation with 1.54 Å wavelength at 40 kV and 40 mA. The detector used is a NaI scintillation counter. The samples are washed with distilled water to remove all dust or mud. After, about 2 g are put in a glass test-tube nearly filled with distilled water and put in a mechanical shaker for about four hours to separate the clay from the rock matrix. The suspended clay-slurry is left to settle for about 10 minutes and then transferred onto to a glass-slide, using a pipette. The sample is left to dry in ambient temperature and humidity. Each sample undergoes three different treatments. First the sample is measured after complete drying (UNT, untreated). After the first measurement the sample undergoes a special glycol treatment inside a closed desiccator where it is left in the ethylene-glycol fume for 24 hours to see if the clay can swell or not, and then it is measured again (GLY, glycolated). Lastly, the sample is heated in a furnace for about 1 hour in 550°C and after cooling, measured again (HIT, heated). The set of three measurements is then viewed superimposed using special software for X-ray diffraction data display (Bruker, Diffra-Eva). Such analyses are useful in determining the alteration zones along with other index minerals found in binocular and petrographic analysis. The XRD analyses of clay minerals in well SV-26 are found in Appendix III.

Fluid inclusion analysis
The analysis offers direct information on the temperature during the formation of the hydrothermal minerals and was used in this report (along with the temperature of first appearance of alteration minerals and the formation temperature) for the interpretation of the thermal condition of the geothermal system. The examination is conducted by gradually heating up the sample using micro thermometry, to the homogenization temperature of the fluid inclusions, so that the bubble inside the fluid inclusions, trapped during crystallisation, disappears. Fluid inclusions were identified from specific depths and mostly quartz was selected for the fluid inclusion studies.

Interpretation of geophysical logs
Neutron logs: The physical basis of measurements of neutron logs is the scattering and capture of neutrons; the main purpose is to estimate the formation porosity (Steingrímsson, 2011). This is useful in the identification of intrusions, which are usually compact compared to the intruded rock formations.

Calliper log measures the diameter of the well as a function of depth using a logging probe with arms placed symmetrically around it (Steingrímsson, 2011). Indications of wider areas in the well can point to the locations of soft formations or fractured areas where the walls of the well are easily broken.

Resistivity logs: The specific resistivity of the reservoir rock is the result of two different contributions, the resistivity of the rock matrix and the formation fluid. An igneous rock matrix is generally a poor electrical conductor at geothermal temperatures (Mostaghel, 1999). Therefore, an igneous rock with considerable porosity or fluid filled vesicles will show rather low resistivity. The resistivity graph will show lower resistivity in the aquifer zones.

Gamma log measures the natural gamma radiation, used to determine the clay content in rocks. Investigations in Iceland show, however, that the gamma ray activity in volcanic rocks is related to the SiO_2 content of the rock and can, consequently, be used to identify rocks of evolved compositions (Mostaghel, 1999).

2.3 Stratigraphy of well SV-26

The lithology of well SV-26 corresponds well with the lithology model made by Franzson (2017). The model is based on cutting analysis from older wells in the Svartsengi area and shows how interglacial lava series are intersected by hyaloclastite horizons, including pillow basalt, breccia, tuffs and reworked tuffs. Due to total loss of circulation in well SV-26, no drill cuttings were retrieved below 1394 m. In addition, several gaps of cutting retrievals existed at shallower depths, due to loss of circulation during

drilling. Geological information below 1394 m depths is exclusively based on the geophysical logs and the drilling parameters. These correlate fairly well with Weisenberger et al. (2016). An overview of the lithology, alteration and alteration mineral distribution is shown in Figure 8.

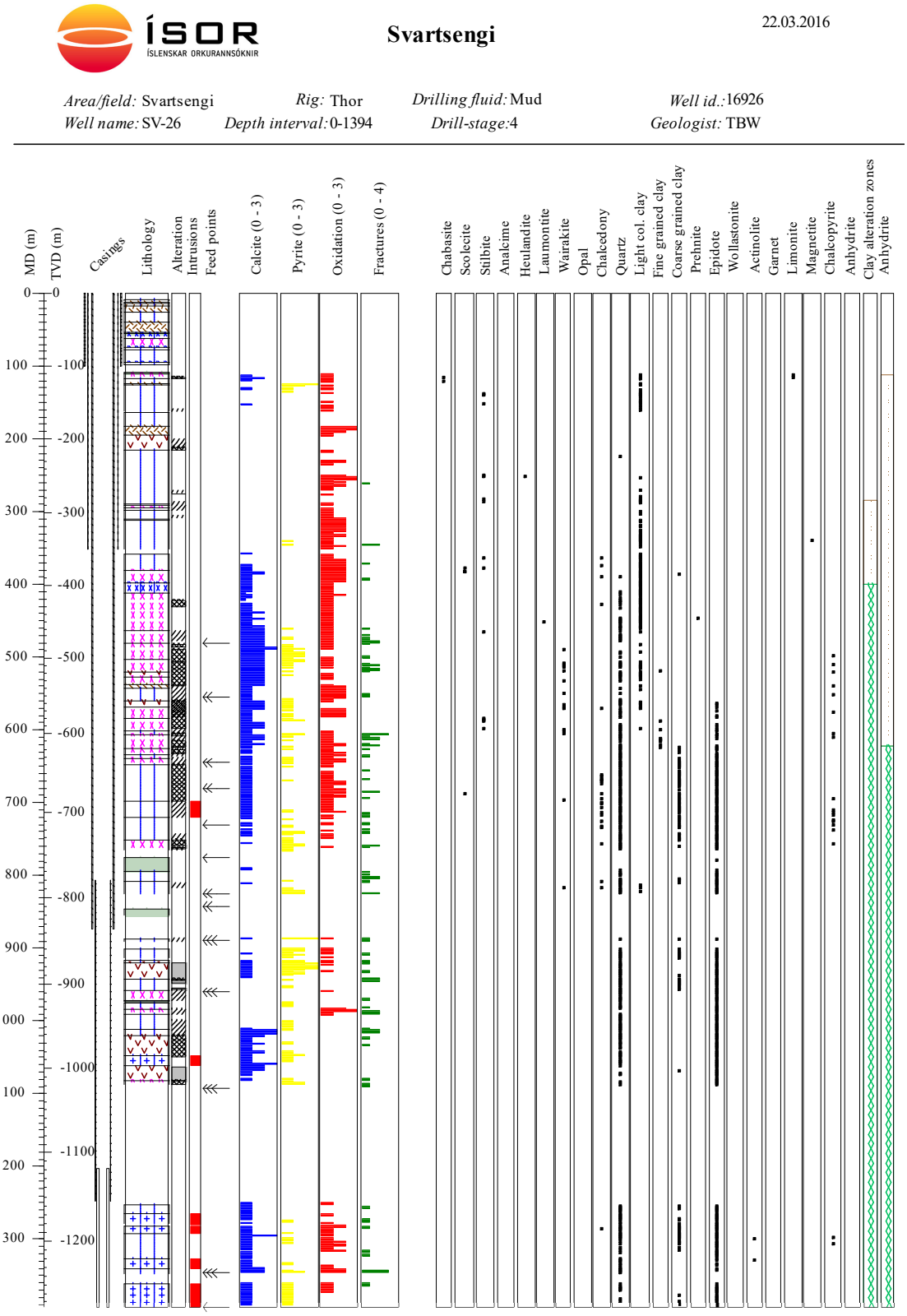

FIGURE 8: An overview of alteration and lithology in well SV-26 from 0–1394 m measured depth. Please include further explanation

8–10 m: Lava
Fine- to medium-grained well crystallized basalt. Occasional plagioclase micro-phenocrysts are seen. Grains are dark in colour, dense and fresh. Red scoria fragments are mixed in.

10–12 m: No cuttings

12–14 m: Scoria
Lava boundary. Mostly red and foam-like scoria grains observed. Tuff mixed in and broken plagioclase crystals.

14–18 m: Lava
Red scoria and tuff fragments with occasional light grey and fine-grained basalt.

18–26 m: Scoria
Scoria mixed with crystallized basalt grains.

26–40 m: Lava
Fine- to medium-grained light grey coloured and dense basalt grains. Few plagioclase and clinopyroxene micro-phenocrysts. Abundance of grains are crystallized and oxidized.

40–54 m: Scoria
Red and foam-like scoria. Crystallized basalt grains mixed in along with few tuff grains. Large plagioclase micro-phenocrysts.

54–56 m: No cuttings

56–62 m: Pillow basalt
Scoria and orange coloured grains mixed with cement.

62–74 m: Basalt breccia
Breccia formation. Increase in black, fresh tuff grains. Basaltic grains are very fine-grained and poorly crystallized. Occasional plagioclase micro-phenocrysts occur.

74–78 m: Pillow basalt
Less tuff grains than previous.

78–94 m: Lava
Abundance of euhedral pyrite crystals. Dark grey, medium-grained and plagioclase-rich basaltic grains. Some grains are somewhat porous and also green grains can be found. These are mixed with oxidized grains.

94–98 m: Pillow basalt
Glassy and porous grains containing green and yellow fillings. Fine-grained clay noticed and abundance of calcite. Cuttings are with occasional well-crystallized basaltic grains. Highly altered olivine micro-phenocrysts are noticed.

108–110 m: No cuttings
Only cement

110–118 m: Breccia
Basaltic breccia. Cement fragments are still present. Secondary minerals like calcite and limonite are found within pores. Fragments are slightly oxidized.

118–124 m: Lava
Fine-grained basaltic lava with olivine. Alteration minerals found inside pores include clays, thomsonite, and calcite. Upper part of the unit is slightly oxidized.

124–126 m: Scoria
Basaltic scoria. Highly oxidized, pores contain very fine-grained subhedral pyrite crystals.

126–162 m: Lava
Fine-grained plagioclase porphyritic basalt. Very vesicular and partially oxidized. Secondary pore filling minerals are few and including calcite, clays and stilbite. The lithology does not show any sign of alteration.

162–164 m: No cuttings

164–182 m: Lava
Fine-grained plagioclase porphyritic, slightly oxidized basalt. Limited amounts of secondary pore filling minerals are noticed. No signs of alteration.

182–194 m: Scoria
Basaltic scoria with foam-like texture. Highly oxidized.

194–216 m: Tuff
Greenish basaltic tuff. Shallower samples are mixed with scoria. The upper tuff units are unaltered, in contrast to the lower unit which shows signs of low to medium alteration.

216–290 m: Lava
Fine- to medium-grained basalt with very limited appearance of vesicles. Few secondary minerals are observed, including quartz, clay, zeolites (stilbite, scolecite). The middle part of the basalt formation shows strong oxidation (possibly 2 lava flows).

290–292 m: Breccia
Basaltic breccia, slightly altered.

292–294 m Lava
Fine- to medium-grained basalt. It is slightly altered and oxidized.

294–298 m: Breccia
Basaltic breccia, slightly altered and oxidized.

298–310 m Lava
Fine- to medium-grained basal. It is fresh and slightly vesicular. Vesicles are coated with clays.

310–312 m: Breccia
Basaltic breccia. Slightly altered and oxidized.

312–352 m: Lava
Fine- to medium-grained olivine-bearing basalt. It shows strong, grain selective oxidation. Alteration minerals are mostly clays which replace the olivine. Some pyrite is observed.

352–358 m: No cuttings

358–380 m: Lava
Fine- to medium-grained (sometimes almost glassy) basalt. It is quite dense. Olivine crystals are mostly oxidized or altered to clay. Oxidation is also prevalent in the groundmass. The main alteration minerals

are calcite and clay but stilbite and other zeolites are also found.

380–398 m: Breccia
Fragments with a variety of crystallinity, mostly porous tuff and fine-grained basalt. Increased alteration due to higher glass content. Variety of clays, unidentified zeolites, calcite and aragonite in few places.

398–412 m: Glassy basalt
Increase in crystallinity, more homogeneous and less porous and oxidized than above. Dark grey with few secondary minerals.

412–464 m: Breccia
Porous tuff, glassy basalt and fine-grained basalt. Quartz is often found below 410 m and in every sample below 448 m.

464–480 m: Breccia
A mixture of blue-green tuff and light-grey basalt. The tuff fragments have been partially oxidized and the pores and fractures are mostly filled with alteration minerals such as calcite, clay and quartz. The small pores in the basalt are mostly filled with dark green clay.

480–504 m: Breccia
There is an increase in the amount of tuff that appears to be white due to alteration. Rich in secondary minerals, but mostly calcite and quartz. Wairakite is found in fractures below 490 m. Minor fine-grained dark, plagioclase porphyritic basalt fragments are mixed in. The plagioclase phenocrysts show signs of alteration.

504–520 m: Breccia
Colourful, tuff-rich breccia, green, white and oxidized. Minor black, dense, fine-grained basalt.

520–528 m: Tuff
Greenish tuff cemented together, mostly with calcite.

528–538 m: Breccia
Same tuff as above mixed with dark grey dense, plagioclase porphyric, fine-grained basalt that is slightly oxidized.

538–542 m: Scoria
Oxidized and porous glassy, scoria. Top of lava.

542–560 m: Lava
Grey, fine-grained rather dense and fresh basalt. Small amounts of alteration minerals. The cuttings have much sharper edges.

560–568 m: Tuff
Greenish tuff with white secondary minerals. Mainly calcite, quartz and possible wairakite. Green fine-grained clay is found in pores. Pyrite is observed in small amounts. Epidote appears for the first time at a depth of 564 m.

568–582 m: Breccia
Greenish tuff with light-grey and dark fine-grained basalt. Some of the fine-grained basalt fragments are oxidized. Some zeolites are found in pores but other are being transformed into other higher temperature alteration minerals.

584–602 m: Breccia
Basaltic breccia. Fine-grained breccia that consists of dark-brownish fine-grained basalts and greenish

altered tuff fragments. Rich in secondary minerals (calcite, stilbite, clays, zeolites).

602–606 m: Lava
Fine-grained basalt. Fine-grained basalt with lots of vesicles, which appears to be partially glassy. The cuttings are coarser grained than previous samples. Minor greenish altered tuff is mixed in. It is rich in secondary minerals, which include zeolites and quartz (euhedral). Several small fracture fills are observed.

606–626 m: Breccia
Very heterogeneous basaltic breccia. Fine-grained breccia that consists of dark-brownish fine-grained basalt that often are highly vesicular and greenish altered tuff fragments. Fragments are slightly altered and oxidized. Olivine phenocrysts are altered to clay minerals. Secondary minerals include calcite, zeolites, quartz, clays, pyrite, and epidote. Rich in fractures filled with secondary minerals.

626–634 m: Breccia
Very heterogeneous basaltic breccia. Fine-grained breccia that consists of dark-brownish fine-grained basalt which often are highly vesicular, greenish altered tuff fragments, and light coloured small- to medium-grained crystalline olivine-bearing rock fragments.

634–640 m: Lava
Fine-grained basalt. Plagioclases porphyritic in places, vesicular and slightly oxidized, pores are filled with secondary white minerals. Small amount of light coloured fine-grained fragments that contain plagioclase and olivine phenocrysts of variable alteration degrees. White secondary pore filling minerals and epidote.

640–648 m: Breccia
Very heterogeneous basaltic breccia. Fine-grained breccia that consist of dark-brownish, fine-grained basalts that often are highly vesicular, greenish altered tuff fragments, and light coloured fine- to medium-grained crystalline rock fragments, that contain fresh to altered olivine.

648–698 m: Lava
Fine-grained basaltic lava. Medium- to strongly-altered, light-dark, slightly reddish, very fine-grained olivine-bearing basalt. In parts plagioclase porphyritic. Appears to be massive, but vesicles and pore space appear irregular in higher quantities. Low-degree of oxidation is observed throughout the unit, whilst the oxidation is patchy and not homogenously distributed within the rock. Very rich in epidote (present in every sample). Additional secondary minerals include calcite, quartz (including euhedral quartz) and clays.

698–720 m: Lava
Fine- to medium-grained basaltic lava. Similar lava fragments as within the lava unit above, but mixed with minor, non-altered medium-grained dark basalt fragments. Rich in epidote and quartz (both euhedral and anhedral).

720–752 m: Lava
Unaltered fine- to medium-grained basalt. Lava unit is coarser-grained than previous unit. Basalt fragments are dark and unaltered. Only limited pore space, but most of the pores are lined with epidote and quartz. Epidote also occurs as replacement phase of primary minerals. Additionally, pyrite, chalcopyrite and chlorite occur. At a depth of 732m, large (1 cm) quartz aggregate with disseminated pyrite are observed.

752–765 m: Breccia
Mixture of quartz aggregates with disseminated pyrite (euhedral and anherdal), highly altered basalt and fine- to medium-grained fresh basalt fragments. Cuttings are large (up to 5 mm) and individual fragments are semi-rounded. At 765 m a total loss of circulation happened.

765–766 m: No cuttings
Loss of circulation.

776–794 m: No cuttings
Cement only.

794–808 m: Lava
Fine-grained basalt: dark fine-grained basaltic lava. Relatively massive with only limited pore space. Epidote is the dominant secondary mineral, with minor quartz and pyrite. Several small mineralized fractures.

808–826m: Lava
Fine- to medium-grained basalt. It is coarser-grained than previous lava unit. Epidote is the dominant secondary mineral. Additional quartz and pyrite appear in the deeper parts of the unit in larger quantities. Several small mineralized fractures.

826–888 m: No cuttings
Loss of circulation.

888–890 m: Lava
Fine-to medium-grained basalt. The slightly greyish cuttings are slightly altered and oxidized. They contain a large amount of pyrite. Olivine phenocrysts are altered to clays/chlorite. Additional secondary minerals are quartz, epidote, chlorite, and calcite. Thereby pyrite and quartz are associated as disseminated pyrite in quartz. One quartz fracture was detected.

890–902 m: No cuttings
Loss of circulation

902–914 m: Lava
Fine-to medium-grained basalt. The slightly greyish cuttings show a slight sign of alteration and oxidation. Olivine, which occurs sparsely, is altered to chlorite. The unit contains a high content of pyrite, whereas pyrite is often disseminated within whitish quartz fragments. Additional secondary minerals are epidote, chlorite and calcite. One fracture fill with epidote was detected at 908 m. Cutting fragments get finer with increasing depth.

914–917 m: No cuttings

917–920 m: Lava
Fine-to medium-grained basalt. The slightly greyish cuttings are slightly altered. Secondary minerals include quartz, pyrite and epidote.

920–942 m: Tuff
Highly altered whitish to slightly greenish hyaloclastite. It contains a very high amount of quartz fragments that are disseminated with pyrite. In addition, minor massive pyrite aggregates are found. Some minor oxidized grains occur within the upper part of the stratigraphic unit. Upper cutting samples of this unit are mixed with fine- to medium-grained basalt, whereas the basalt content decreases with depth. Secondary minerals include quartz, pyrite, epidote, and minor calcite.

942–958 m: Lava
Fine-to medium-grained basalt. Sharp contact with the previous basaltic tuff unit. The slightly greyish to brownish cuttings are slightly altered on top of the stratigraphic unit. Cutting samples contain a high content of epidote. Addition secondary minerals are minor quartz, pyrite, and chlorite. Hyaloclastite grains are mixed in variable concentrations.

958–974 m: Breccia
Basaltic breccia. Fine-grained cuttings that consist of similar proportions of fine-grained basalt and basaltic tuff fragments. The whitish basaltic tuff is highly altered, whereas the brownish to reddish basalt fragments are only slightly altered. It contains a high content of epidote. Additional quartz and chlorite are present.

974–976 m: No cuttings
Only cement

976–984 m: Lava
Fine-grained basalt. It is slightly altered and grains are slightly reddish in colour. Some grains are highly vesicular and vesicles are in general totally filled with secondary minerals. Epidote is the dominant alteration mineral. In additional, quartz occurs in variable quantities. Pyrite is found in the upper part of the unit. Minor amount of altered basaltic tuff fragments is found.

984–990 m: Breccia
Highly oxidized basaltic breccia. Very heterogeneous unit that is composed of reddish fine-grained and altered components, darkish only slightly altered fine-grained basalt fragments that are sometimes vesicular. Epidote is found in minor amounts.

990–1012 m: Lava
Fine- to medium-grained basalt. The crystalline and massive basalt fragments which are slightly altered are very bright and greyish and whitish in colour. With depth the cutting colour is getting darker. Rich in epidote and quartz, which is also found as fracture fill. Additionally, pyrite is found in minor amounts. Small amounts of oxidized fragments are mixed in. Sample at 1008 m has a high content of epidote and quartz.

1012–1020 m: Lava
Fine- to medium-grained basalt. Similar to the unit above. But in addition it contains a high content of whitish mono-mineral calcite.

1020–1048 m: Hyaloclastite
Whitish to greenish basaltic tuff. Glass fragments are greenish and are only slightly altered. Glass fragments are semi-rounded and sit within a whitish matrix. It contains a high content of secondary minerals, including epidote (euhedral in places), quartz, and calcite. In addition, pyrite occurs in small amounts. Minor amount of basaltic lava fragments is mixed in.

1048–1062 m: Intrusion/dike
Medium-grained basalt. Fresh, crystalline basalt that is black in colour. Minor amounts of secondary minerals, including epidote, quartz, calcite and pyrite.

1062–1082 m: Hyaloclastite
Basaltic tuff. Whitish to slightly greenish basaltic tuff. In contrast to the previous basaltic tuff, the cuttings are finer-grained and the fragments are highly altered. It contains a high content of secondary minerals, including epidote (euhedral in places), quartz, calcite, and chlorite.

1082–1088 m: Breccia
Basaltic breccia that consists of basaltic tuff fragments and slightly reddish fine-grained basalt fragments. Fragments are in general altered and epidote occurs frequently as a major alteration product. Additional pyrite (incl. euhedral pyrite) is found in higher quantities. Cuttings are coarser-grained than hyaloclastite unit above.

1088–1252 m: No cuttings
Loss of circulation

1252–1564 m: Lava
Fine to medium-grained fresh basaltic lava. Fresh holocrystalline and massive basalt, which is slightly reddish to greyish in colour. It contains some minor amounts of oxidized grains. Upper part of the unit is mixed with cement fragments. Epidote and quartz occur in large quantities, and euhedral crystals are also common. Additional chlorite aggregates are found and minor calcite.

1264–1279 m: Possible intrusion/dike
Medium-grained fresh basalt. Fresh holocrystalline and massive basalt, which is very dark (blackish with a reddish tint) in colour that marks a sharp colour contact with the previous lava unit. Oxidized grains are found sporadically and particularly in the deeper part of the unit. Minor cement fragments are present. Upper part of the unit is mixed with cement fragments. Epidote and quartz are the dominant secondary minerals, but occur in much lower amounts.

1279–1282 m: No cuttings
Only cement

1282–1292 m: Possible intrusion/dike
Medium-grained fresh basalt. Holocrystalline, massive basalt, which is grey in colour and has a reddish tint. It is fresh but shows a higher degree of oxidation, whereas the oxidation decreases with increasing depth. Minor cement fragments are present. Epidote, quartz and chlorite are the dominant secondary minerals with minor calcite being present. Within the lower part of the unit, minor large (> 3 mm) whitish aggregates are observed, which contain black inclusions that show a preferred orientation.

1292–1326 m: Lava
Fine- to medium-grained fresh basalt. Massive basalt with minor vesicles within the upper part of the unit, and occasionally vesicles are observed in samples within the lower unit. It is dark-greyish and the individual depth intervals are slightly oxidized. Epidote, quartz and chlorite are the dominant secondary minerals with minor calcite. In the sample at 1298 m a dark, slightly greenish secondary fibrous mineral is found that forms a radiating aggregate around quartz (possible actinolite). Occasionally minor pyrite is observed. The content of secondary minerals decreases with increasing depth. Minor large (> 3 mm) whitish aggregates are observed, which contain black inclusions that show a preferred orientation.

1326–1340 m: Possible intrusion/dike
Medium-grained fresh basalt. Holocrystalline, massive basalt, which is dark-greyish to black in colour. Very limited content of secondary minerals that includes epidote, quartz, and calcite. Chlorite is the dominant secondary mineral with minor calcite being present. Minor large (>3 mm) whitish aggregates are observed, which contain black inclusions (actinolite?) that show a preferred orientation.

1340–1348 m: Lava
Fine- to medium-grained basalt. The fresh basalt is dark-greyish in colour and contains numerous deep-red totally oxidized fragments, where the dark-greyish fragments do not show any sign of oxidation. Secondary minerals include epidote, quartz, calcite and pyrite.

1348–1362 m: No cuttings
Total loss of circulation

1362–1394 m: Possible intrusion/dike
Medium-grained basalt. The fresh and massive holocrystalline basalt is dark-grey in colour, whereas minor variations (greenish and reddish) are observed. Small amounts of fine-grained basalt fragments are present in variable proportions. Secondary minerals included epidote, quartz, calcite, and pyrite Minor large (mm—size) whitish aggregates are observed within the upper part of the lithological unit, which contains black inclusions that show a preferred orientation.

1394–2537 m: No cuttings
Total loss of circulation

2.4 Intrusions

Intrusions are emplacements of magma into pre-existing rocks. As the subterranean magma slowly cools it gives time for the crystals to grow thus, they usually show relatively coarser textures compared to the host rock. Intrusive rocks are characterized by their massive, compact nature and appear fresh in comparison to the surrounding lithology, and are sometimes marked by oxidation near their margins (Worku, 2012).

No intrusions were observed above 1000 m depth in well SV-26, except at the depth interval between 698 and 720 m were a lava unit contained fresh medium-grained basalt fragments, which may indicate the presence of dikes/feeder-dikes. In contrast, several possible intrusions and/or dikes have been detected in deeper parts of the well (1048–1062, 1264–1279, 1282–1292, 1326–1340, and 1362–1394 m). This approximately coincides with the depth interval from 1100 to 1300 m that is well known for high amounts of intrusions within the Svartsengi geothermal field (Franzson, 1990). However, a lack of drill cuttings below 1300 m from most wells in Svartsengi, results in limited knowledge of locations of intrusions at greater depths (Gudjónsdóttir et al., 2015).

Spikes in the gamma log which often also show in the neutron and resistivity logs can be markers of possible intrusions. This are indicatives for evolved rocks that are low in porosity. This is noticed at following depth intervals: 1420–1440, 1540, 1560–1580, 1740, 1755, 1780, 2120–2140, 2180–2235, and 2310–2400 m.

2.5 Geophysical logs

Geophysical logs (Weisenberger et al., 2016) for each phase can be found in Appendix I (Figures 1-4).

Phase 1
Temperature log. Maximum temperature measured was about 60°C and as no loss of circulation had been reported and no indication of feed zones is noted in the temperature log.

XY-calliper log. The log shows a cave from 200–215 m depth which is associated with the tuff horizon at similar depth.

Resistivity log. The small peaks in resistivity at 215–250 m correlate with a fresh, massive basalt lava formation.

Neutron-neutron log. Is rather flat and does not reveal any details in a well of this wide diameter and full of thick mud.

Phase 2
Temperature log. Shows a small step in temperature at 480 m and larger step at 550 m. Both steps indicate an inflow into the well. The water table is located at shallower depth (430 m), as indicated by the neutron and gamma logs as well as the resistivity log. A small pivot point appears at 640 and coincides with a previously reported feed point, but a large amount of the injection (and the inflow) flows towards the bottom of the well and flows out of the well at 860–870 m depth.

XY- calliper log. Shows large variations of well diameter along the depth interval. In general, it seems that the washout is higher within the hyaloclastite formations than in the lava formations. A large caving is located between 550 and 590 m. This coincides to a hyaloclastite formation with thin lava formations both above and below the hyaloclastite. A possible intrusion was logged at around 700 m. The calliper log shows a resistant unit at similar depth and as well as small caving structure below and above the intrusion. Within the lowest part of the well the calliper log shows a sharp contraction at 850 m within

a clear washout zone above from 825 to 850 m. At similar depth a loss of circulation occurred and the drill bit got stuck several times.

Neutron-neutron log. Can be divided in a shallower interval down to about 600 m and a deep interval below. The transition is marked by a sharp increase in neutron count rate at 600 m, indicating lower porosity rocks. Above 600 the lithology is characterized by a hyaloclastite formation and higher porosity. Small spikes in the neutron log within the hyaloclastite formation are probably associated with brecciated layers and/or basaltic dikes within hyaloclastite. A sharp peak neutron log at 540 m that coincides with the upper contact zone of an intercalated lava flow within the hyaloclastite formation. The abrubt increase in the neutron log at 600 m is not directly associated with a significant change in lithology according to the drill cuttings. The formation boundary of the hyaloclastite and lava formations is at 648 m. However, the lower part of the hyaloclastite formation (> 600 m) contains intercalated lava units. This transition zone from the hyaloclastite to the lava formation is possibly associated with the sharp increase in the neutron log. Below 750 m the neutron logs shows a large scattering, which may reflect the brittle formations within the graben structure.

Gamma log. Shows an increase at 650 m and coincides with a postulated change in alteration to the epidote alteration zone.

Resistivity log. Shows a low-resistivity cap within the shallow depths down to about 640 m. The increase in resistivity at 650 m coincides with the appearance of epidote, which starts to occur in every sample below 634 m. The appearance of epidote and the increase in resistivity are an indication for the transition of the mixed layer clay alteration to the chlorite-epidote alteration zone at the depth around 640 m.

Phase 3

Temperature log. The logging program started with a pumping rate of Q = -15 L/s. The flow screened the feed zones at 900 and 950 and a good feed zone is clearly seen at s 1090–1100 m. The well is relatively tight below 1100 m but the temperature log shows a minor down flow in the well towards feed zones at 1235 m. Maximum temperature showed about 110°C at 1245 m. At 1090 m depth a total loss of circulation occurred. This took place in a basaltic breccia formation where epidote occurs frequently as a major alteration product, in addition to quartz, calcite, and chlorite. Abundance of pyrite was also found in the cuttings just before the loss.

XY-calliper log. It shows wash-out, even caving, below the casing which was set at 873.5 m depth. The well was rather elliptic down to about 985 m, but less elliptical from there on and down hole. However, at about 1090 m a clear, moderately narrow, yet substantial wash-out is observed, correlating to the fracture causing the total circulation loss observed at this depth and quite possibly a fault zone, indicated by the abundance of high-temperature alteration minerals and pyrite/calcite.

Neutron-neutron, gamma and resistivity logs. NN and gamma logging was measured to a depth of 1235 m. The gamma log shows clearly that the rock formations so far penetrated are of a basaltic geochemical composition. The NN and resistivity correlate fairly well, for example at the interval between 940–980 m, which consists mostly of basaltic lavas and some breccia, followed by highly oxidized breccia, which again is followed by lava down to about 1020 m and subsequently hyaloclastite rocks. From 1090 m depth no cuttings are available and it is hardly possible to interpret the geophysical logs according to rock formation. However, there do not appear to be any intrusive rocks from 1090–1235 m depth.

Phase 4

Temperature log. Shows major inflow at 1346 m depth, same depth as the TLC happened and minor inflow at 1450 m. The log shows some flow out of the well at 2120 and 2250 m, but the main outflow is at 2430 m about 100 m above the bottom. At this depth the drilling parameters indicate the penetration of a fault. The temperature profile indicates that practically no down flow continues past the feed zone at 2428 m indicated by the temperature rise from ~50°C at 2400 to ~150 at 2500 m.

The XY-calliper. A major cave is at 2060 m depth but there is no sign of a feed zone at this depth according to temperature logs. Additional small caves are identified at 1346, 1550, 1580, 1650, 1900, 2210, 2380, 2428 m depth.

Gamma log. Shows only limited variations. Gamma peaks appear at depth of 1420, 1440, 1540, 1560, 1580, 1740, 1755, 1780, 2120–2140, 2180–2235 and 2310–2400 m and may indicate lithological units with higher gamma radiation and may reflect higher fractionated dikes or intrusions.

Neutron-neutron log. Shows only minor variations. Notable is the high neutron count in the depth interval from 2235 to 2310 m, which may reflect a lower porosity layer in between the dike/intrusions above and below this depth interval. Further small peaks within the neutron log are observed, which often coincide with peaks of the resistivity logs and may reflect thin, low porosity layers.

Resistivity log. The resistivity curves show a gradual increase with increasing depth from about 10 Ωm to about 60 Ωm for the 64''log. The oscillation of the resistivity logs and the location of observed peaks (e.g. at depth of 1320, 1540, 1580, 1870, 2250 and 2350 m) mimic peaks observed also in the neutron log.

2.6 Hydrothermal alteration

A summary of the distribution of alteration minerals in well SV-26 is presented in Figure 8. A regular progressive hydrothermal alteration with increasing depth was noticed from the alteration mineral assembly in well SV-26 (Table 2). Such depth and temperature controlled mineral alteration zoning is well known in Icelandic hydrothermal systems (Kristmannsdóttir and Tómasson, 1978; Franzson 1998; Weisenberger and Selbekk, 2009). Low-temperature minerals, like fine-grained clay and zeolites occur at shallower levels, whereas high-temperature minerals, like epidote and coarse-grained clay appear at deeper levels in the well. The production casing is located at 1250 m and based on the mineral assembly, the production casing was extended well into the geothermal reservoir, with abundance of epidote (> 230–250°C) noticed in cutting samples at that depth. Epidote was first observed at 564 m depth, whereas below 626 m epidote was frequently observed in the majority of the cutting samples. In samples at 1298 m and 1328 m, a fibrous dark greenish mineral has been observed, but due to the very small grain size there is still unclear whether it is actinolite or not. No drill cuttings were available for analysis below 1394 m depth due to total loss of circulation.

TABLE 2. An overview of the depth of occurrence of alteration minerals in SV-26

Alteration mineral	SV-26 (m)
Calcite	112
Zeolites appear	116
Quartz	390 (224)
Wairakite	490
Epidote	564
Low-T zeolites disappear	584
Actinolite*	1298
*uncertain	

The upper boundary of cap-rock of the geothermal reservoir is found at about 380 m in well SV-26. This is at about the same depth as in well SV-25 (360 m) (Gudjónsdóttir et al., 2015). However, the shallower cap-rock formation does not show any sign of alteration but alteration suddenly appears at a depth of about 465 m. Increased calcite content is observed at depths below 380 m (Figure 8). High oxidation was noticed in the drill cuttings from SV-26. The oxidation was especially noticed in the upper 700 m of the well, associated with lava formations, breccia and pillow basalts (Figure 8). Within

the depth interval between 700 and 1100 m, only limited oxidation was observed. However, at the depth interval between 1280 and 1370 m the lithological units show a high degree of oxidation again.

2.6.1 Primary rock minerals in SV-26

Primary minerals are rock forming minerals that form during rock crystallization. The minerals form in a sequence or in sequential groups as detected by the chemistry and physical conditions under which the magma solidifies and it is essential for the classification of the rock. Primary minerals tend to alter and form secondary minerals at conditions of high temperatures, high permeability and fluid activity in a hydrothermal environment (Franzson, 1998; Gebrehiwot, 2010). Hyaloclastite and basaltic lavas are the main rock types throughout well SV-26, and they are mostly composed of volcanic glass, olivine, plagioclase, pyroxene and opaques as the primary minerals.

Volcanic glass is an amorphous (uncrystallised) product formed during the quenching of magma. Glass has low resistance to alteration compared to primary minerals. In well SV-26, clay, smectite and calcite are the common alteration minerals of glass.

Olivine is formed in basaltic rocks. It is the second most vulnerable to alteration after glass. In thin section it is distinguished by its high birefringence, distinctive irregular fracture pattern, lack of cleavage, and its parallel extinction. Along its fractures, the alteration products are usually clay, calcite and chlorite.

Plagioclase is the most abundant primary mineral in igneous rocks. It is easily identified in thin section by its low relief, maximum interference colours are usually first-order grey or white, and twinning distinguishes plagioclase from most other minerals. (Mnzava, 2014). As temperature increases it is progressively altered to clay, calcite, albite, quartz, wairakite, chlorite and epidote.

Pyroxene minerals are significant components of many intermediate and most mafic igneous rocks. Pyroxene is black or dark green in colour and forms prismatic crystals with vitreous lustre and perfect cleavage. Extinction at an inclined angle distinguishes it from olivine as well as its apparent cleavage and light brown colour in plain polarized light.

Opaque minerals do not transmit light in transmitted light microscopes. They are usually magnetite (oxide mineral) in basalt. These minerals were hardly altered throughout the well although often there were signs of oxidation on their edges.

2.6.2 Hydrothermal alteration minerals

Hydrothermal alteration is very informative on various aspects of the geothermal system. It designates the reaction between the reservoir rock and the circulating geothermal fluid, resulting in compositional changes of both the solid and fluid phase as the interaction between rock and fluid usually involves additional and/or removal of major rock-forming components. The factors that usually control alteration in geothermal systems are temperature, rock type, permeability, fluid composition and the duration of fluid-rock interactions (Browne, 1978).

Phase 1
Within the shallow zone of drilling phase 1 (108–352 m) the alteration is very limited and where it appears, it is associated with formation boundaries. Secondary minerals are observed predominantly in the vesicle-rich units. Thereby, clays and various zeolites (stilbite, scolecite, thomsonite) are dominant secondary minerals, with minor calcite, limonite and pyrite, which only occur at limited depth intervals.

Phase 2
Within drilling phase 2 (352–886 m) the secondary mineral inventory is in general higher, but the content depends on the availability of primary pore space. In general, calcite appears throughout the

entire section of drilling phase 2. Zeolites, such as stilbite and scolecite, are found in the lava sequence (< 380 m). They become less frequent in the hyaloclastite formation below the lava formation, which is the cap-rock of the hydrothermal system. Quartz is first detected at a depth of 390 m (beside a single appearance at a shallower depth of 224 m), (Table 2) and implies an alteration temperature increase with depth (180°C). Other secondary minerals include clays, both as fine-grained clay lining in pores and bright-green coarse-grained clay in pores and chalcedony. Zeolites are still found at 458 m but they seem to be overgrown by calcite and quartz. The secondary minerals change with increasing depth and therefore higher formation temperatures can be expected during formation of the secondary minerals. Low-temperature zeolites are rarely seen apart from around 570–584 m, were stilbite seems to be transforming into another secondary mineral, possible quartz. Wairakite was first spotted at 490 m depth which suggests a formation temperature of about 200°C. In the same sample, big plagioclase phenocrysts showed some alteration. This is the exact same depth at which plagioclase alteration was first observed in well SV-18 (Richter et al., 1999). Below 600 m clays and quartz (including euhedral quartz) occur in variable contents. In addition, pyrite disseminated within quartz was observed at depths of 614 and 622 m. The occurrence of disseminated pyrite within quartz is most likely associated with a fracture zone, and may be associated with the appearance of fault A (Figure 9). Epidote (230-250°C) was first observed at a depth of 564 m and below 634 m epidote is found in more or less every sample within drilling phase 2 and throughout the entire section below, where cuttings were retrieved (< 1394 m). Below 600 m, clays appear coarse-grained. However, the clay content seems to be highly variable. The occurrence of disseminated pyrite within quartz that is found at around 750 and 820 m in large quantities is noticeable. At both depths drilling subsequently resulted in a total loss of circulation. This indicates that the fracture zones are located at these depths.

Phase 3

Within drilling phase 3 cuttings were only received between 886 and 1088 m, due to a total loss of circulation. The inspection of alteration minerals indicates that epidote is the dominant alteration mineral. Calcite and chlorite appear in minor quantities. In addition, disseminated pyrite within quartz is observed often at discrete depth intervals (e.g. between 920 and 942 m) and may indicate the penetration of a larger fault during drilling. However, particularly in the depth interval between 700 and 950 m, pyrite is quite common, whereas a significant decrease is observed below 950 m.

Phase 4

The alteration mineralogy is dominated by the high amount of epidote and quartz. Thereby, the content of both minerals is higher in the lava flow unit than in the possible intrusion/dike. Minor amount of chlorite and calcite is found. At a depth of 1278 m some sulphide minerals are observed. In sample 1298 m and 1328 m a fibrous dark greenish mineral has been detected, but due to the very small grain size there is still unclear, whether it is actinolite.

2.6.3 Alteration mineral zonation

Alteration zones refer to the secondary minerals forming and dominating at a certain range of depth within the hydrothermal system, giving clues regarding the formation temperature. Alteration mineral zonation can differ from one geothermal system to another depending on the parent rock, the chemistry and temperature of the area. Icelandic geothermal systems are dominated by basaltic rock formations. From the group of alteration minerals identified in this study, and with respect to their temperature of formation and sometimes the contradictory XRD clay analysis, the alteration zones in well SV-26 will be presented in two separate ways as follows:

1. Zonation depending on the distribution of alteration minerals.

a. *Unaltered zone (0-112 m);* this zone is mainly comprised of surface alteration minerals forming from cold groundwater with temperature ranging from 0 to 40°C.
b. *Smectite –Zeolite (112-622 m);* defined by the first appearance and abundance of smectite clay where at a depth of 82 m it was identified by petrographic analysis in a slight amount (considered as first appearance), confirmed by the XRD analysis at 94 m. Temperature for the

formation of smectite clay is less than 200°C.

c. *Chlorite – Epidote (622-1394 m);* Epidote was first spotted at 564 m but only below 634 m as crystalline epidote.

2. Zonation depending on clay analysis.

Twenty-one samples were chosen for XRD-analysis to locate the transition from smectite, mixed-layer clays and chlorite within the well. X-ray diffractions results (Table 3, Appendix III) indicate that above 400 m smectite is present as the dominant clay mineral. The appearance of mixed-layer clay is detected in a sample at 452 m, indicative of a temperature increase. Analysed samples from depths 506, 566, 600, 678, 758 and 816 m show that chlorite is present. The sample at a depth of 604 m shows that chlorite and mixed-layer clays are both presented. Appearance of mixed layer clay before the chlorite at 452 m is odd because it forms below the chlorite. This could indicate fluctuations in the temperature condition of the geothermal system. This may be caused by cutting mixing or disequilibrium within the hydrothermal system. Based on the XRD analysis two mineral zones can be defined. A smectite zone from 284 to 400 m and a chlorite-mixed layer zone between 400 and 1380 m.

TABLE 3**:** Results of a XRD analysis of clays in SV-26

Sample	Depth (m) (MD)	d(001) OMH Å	d(001) GLY Å	d(002) Å	Type	Remarks
#01	284	13.74	13.84	10.18	SM	
#02	330	13.1	16.5	9.9	SM	
#03	340	12.80	13.59	10.01	SM	
#04	400	12.72	13.44	9.92	SM	
#05	452	12.90/14	14.2	10/12.4	MLC	Peak at 30.1 Å
#06	506	14.59	14.24	7.25	Chl	Unstable chlorite
#07	558	14.4	14.7	9.9	MLC	Peak at 30.9 Å
#08	566	14.68	14.68	7.25	Chl	Unstable chlorite
#09	600	14.5/12.94	14.5	7.20	Chl	Unstable chlorite
#10	604	14.4	14.3	9.9/12.3	Chl/MLC	
#11	626	13.97	14.31	7.18	Chl/MLC	Peak at 30.54 Å
#12	678	14.8		7.3	Chl	Unstable chlorite
#13	758	14.7	7.2		Chl	Unstable chlorite
#14	816	14.8	7.2		Chl	Unstable chlorite
#15	906	14.7	7.2	9.1	Chl/MLC	Peak at 31.3 Å
#16	948	14.6	7.2	9.1	Chl/MLC	Peak at 31.6 Å
#17	958	14.8	7.2		Chl/MLC	
#18	1052	14.4	14.6/7.2	10	Chl/MLC	Peak at 31.2 Å
#19	1068	14.8	15.1	7.3	Chl/MLC	Peak at 32.3/31.2 Å
#20	1300	14.8	15.1	7.3	Chl/MLC	Peak at 33 Å
#21	1380	15		7.3	Chl/MLC	

3. AQUIFERS/FEED ZONES

Feed point locations have been estimated by using the temperature logs and circulation losses. Figure 9 shows faults mapped on the surface in Mt. Thorbjörn, interpolated along their strike for estimation of the depth of penetration of well SV-26. The majority of feed points within the shallower parts (< 1000 m) are associated with the graben structure seen on the surface in Mt. Thorbjörn. Figure 9 shows (from Weisenberger et al., 2016) that the depth intervals where the well path cross-cuts faults A, B, and C are associated with feed zones. In contrast, fault D does not coincide with identified feed zones. But at slightly deeper levels, several feeds zones are detected, which may indicate that the modelled fracture location needs to be amended further east.

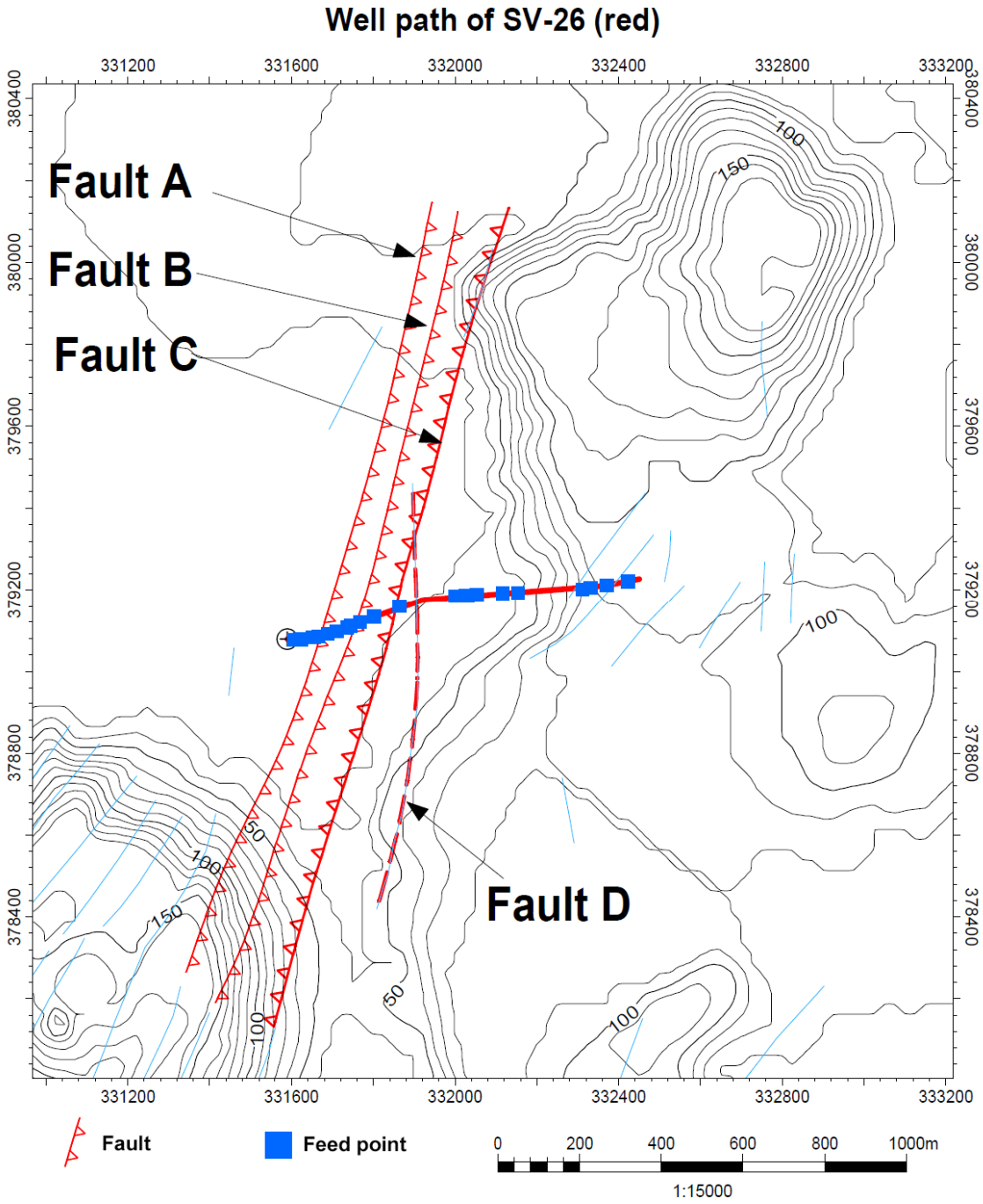

FIGURE 9: Faults mapped on the surface in Mt. Thorbjörn were interpolated along their strike for estimation of the depth of penetration of well SV-26. Feed points are given as blue squares

4. FLUID INCLUSIONS

The study of fluid inclusions shows the temperature of fluid trapped during crystallisation of the minerals, which helps us to interpret the thermal history of the system. By associating the temperatures of fluid inclusions to the present condition of the geothermal system, it is possible to predict whether the system is in equilibrium, cooling or heating. A total of 53 fluid inclusions were studied through micro thermometry in this well within depth intervals ranging from 662-666 m, 808 m, 1046 -1062 m and 1292 m. Of these, 50 inclusions are from quartz samples while the remaining 3 are from calcite and

showed a range of homogenization temperatures (T_h) from 245°C as a minimum temperature to 351°C as a maximum temperature, as described in Table 4 and Appendix II (Figure 1 and Table 4).

The quartz homogenization temperature has a wider range and is higher than the formation temperature showing temperatures above the boiling point curve in the upper section of the well at 664 m and 808 m depth but displays temperatures closer to the mineral alteration curve at deeper depths. The homogenization temperature for the calcite mineral is, however, closer to the formation temperature at around 1292 m depth.

TABLE 4: Fluid inclusion homogenization temperatures

Depth (m) MD	Homogenization temp. (T_h) ranges (°C)	No. of fluid inclusions	Type of crystals
662-666	293 - 341	17	Quartz
808	328 - 351	8	Quartz
1046 - 1062	245 - 291	25	Quartz
1292	261 -263	3	Calcite

Looking at the boiling point curve as plotted and correlated to the other temperature plots (Figure 10), one can conclude that the geothermal system has for most of its lifetime not been in boiling condition at depth, however such condition may have occurred in the uppermost part of the system below 1000 m. The main information the figure shows is that on a geological time scale the geothermal system is on a cooling trend from its hottest conditions in the past.

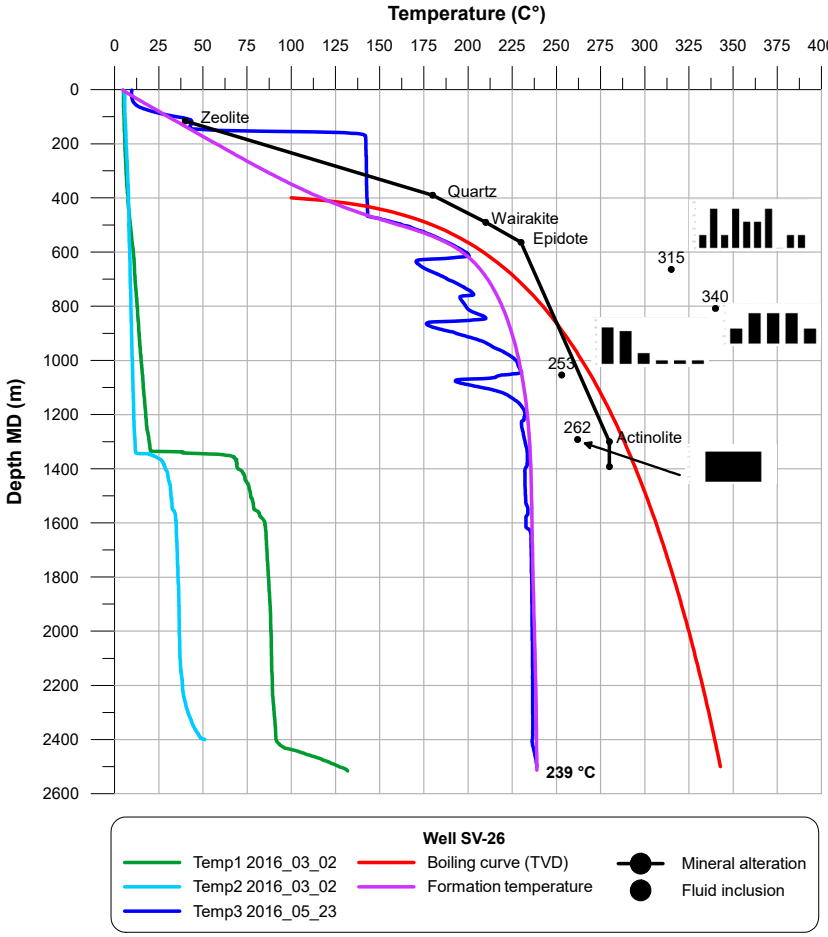

FIGURE 10: Formation temperature, alteration temperature, boiling point curve, homogenization temperatures and logging temperatures of well SV-6

5. CONCLUSIONS

The main conclusions of this report are as follows:

- The stratigraphy of well SV-26, down to 1394 m (MD), is comprised of interglacial lava series which were intersected by hyaloclastite horizons, including pillow basalt, breccia, and tuff. The hyaloclastite cap-rock of the system was reached at depth ~380 m (MD). The upper cap-rock boundary of the geothermal reservoir is therefore, found at about 380 m. However, the shallower cap-rock formation does not show any sign of significant alteration but alteration suddenly appears at a depth of about 465 m.
- The alteration in SV-26 indicates a regular progressive hydrothermal alteration with increasing depth based on the alteration mineral assembly in the well. Epidote (230–250°C) was first spotted at 564 m, and was consistently present below 634 m as crystalline epidote.
- Three alteration zones were observed: Unaltered zone (0-112 m), smectite-zeolite zone (112-622 m) and chlorite-epidote zone (622-1394 m).
- Several feed points were observed according to temperature loggings in the well with the largest at around 889, 960, and 1093 m, located behind the production casing, and in the production part the main feed zones are at 1346 and 2428 m.
- The estimated formation temperature for well SV-26 is 239°C and is in the narrow range of 235-245°C which relates to the fluid temperatures found in wells drilled at Svartsengi geothermal high-temperature field.
- A comparison shows that the alteration minerals formed at considerable higher temperatures than shown by the present formation temperature and would suggest that the reservoir is gradually cooling on a geological time scale. While temperatures at about 600 m may have been near boiling at one time, the geothermal system has probably never reached boiling conditions in deeper parts, and remained water dominated.
- Consistent data, resulting from micro-thermometry analyses done on fluid inclusions found in quartz crystals, show some abnormally high temperatures above 1000 m reaching 351°C around 800 m, which cannot be explained at the moment and should be further addressed. However, it shows conclusively that the Svartsengi system had an earlier hotter environment and has cooled.
- It is important to note that the temperature loggings and mineral sequences of the exploration well SV-26 do not show any evidences of temperature reversal in this part of the production field, which implies that the Svartsengi geothermal system may possibly extend further to the east than previously believed.
- It is important to monitor SV-26 in the future as the temperature will likely rise further still, possibly to temperatures above the Svartsengi average. Such a temperature increase is observed away from Svartsengi to the west towards the Eldvörp geothermal system.

ACKNOWLEDGEMENTS

I thank my supervisor Dr. Björn S. Hardarson for his patience, guidance and for the great time offered during fieldwork and his help in the creation of this report. Sigurdur S. Jonsson for XRD work. I would like to express my gratitude to all UNU staff for their assistance and ÍSOR staff for taking time to share their skill and knowledge with me. Special thanks to Lúdvík Georgsson for giving me the opportunity to attend the UNU Geothermal Training Programme. I gratefully acknowledge HS Orka for allowing me access to data regarding SV-26.

REFERENCES

Björnsson, S., Gudmundsdóttir, I.D., and Ketilsson J. (eds.), 2010: *Geothermal development and research in Iceland*. Orkustofnun, Reykjavík, 39 pp.

Browne, P.R.L., 1978: Hydrothermal alteration in active geothermal fields. *Annual Reviews of Earth and Planetary Science, 6,* 229-250.

Franzson, H., 1990: *Svartsengi. Geological model of the high-temperature, geothermal reservoir and its surroundings.* Orkustofnun, Reykjavík, report OS-90050/JHD-08 (in Icelandic), 41 pp.

Franzson, H., 1995: Geological aspects of the Svartsengi high-temperature field, Reykjanes Peninsula, Iceland. *Proceedings of the 8th International Symposium on Water-Rock interaction, Vladivostok, Russia, 1995*, 497-500.

Franzson, H., 1998: Reservoir geology of the Nesjavellir high-temperature field in SW-Iceland. *Proceedings of the 19th Annual PNOC-EDC Geothermal Conference, Manila*, 13-20.

Franzson, H., 2017: *Svartsengi – Eldvörp. A conceptual geological model of the geothermal reservoir.* Prepared for HS Orka, report ISOR-1017/017, 69 pp.

Gebrehiwot Mesfin, K., 2010: *Subsurface geology, hydrothermal alteration and geothermal model of northern Skardsmyrarfjall, Hellisheidi geothermal field.* University of Iceland, MSc thesis, UNU-GTP, report 5, 65 pp.

Georgsson, L.S., 1984: Resistivity and temperature distribution of the outer Reykjanes Peninsula, Southwest Iceland. *54th Annual International SEG Meeting, Atlanta, Expanded Abstracts*, 81-84.

Gudjónsdóttir, S.R., Tryggvason, H., Gunnarsdóttir, S.H., Níelsson, S., Weisenberger, T.B., Egilson, TH., and Jónsson, S.S., 2015: *Well report – SV-25. Drilling of well SV-25 from surface down to 2004 m and geothermal studies during the drilling of the well.* ÍSOR - Iceland GeoSurvey, Reykjavík, report ÍSOR-2015/077, 263 pp.

Hardarson, B.S., Fitton, J.G., and Pringle, M.S., 1997: Rift relocation - a geochemical and geochronological investigation of a paleo-rift in northwest Iceland. Earth Planet Sci. Lett., 153, 181-196.

Hjartarson, Á. and Saemundsson K., 2014: Bedrock map of Iceland, 1:600 000. ÍSOR – Iceland GeoSurvey, Reykjavík.

Jakobsson, S.P., 1979: Petrology of recent basalts of the Eastern Volcanic Zone, Iceland. *Acta Naturalia Islandica*, *26,* 103 pp.

Jakobsson, S.P., Jónsson, J., and Shido, F., 1978: Petrology of the western Reykjanes Peninsula, Iceland. *J. Petrology, 19-4,* 669-705.

Jóhannesson, H., 1989: The geology of the Reykjanes Peninsula. In: Egilsson, K. (editor), *The nature of the southern Reykjanes Peninsula.* Náttúrfraedistofnun Íslands, Reykjavík (in Icelandic), 13-22.

Jóhannsesson H. and Sæmundsson K., 1999: Geological map of Iceland, 1:1 000 000. Icelandic Institute of Natural History, Reykjavik, 1999.

Jónsson, J., 1978: *A geological map of the Reykjanes Peninsula*. Orkustofnun, Reykjavík, report OS/JHD 7831 (in Icelandic), 333 pp and maps.

Kristmannsdóttir, H. and Tómasson, J., 1978: Zeolite zones in geothermal areas in Iceland. In: Sand, L.B., and Mumpton (editors), *Natural zeolites, occurrence, properties, use*. Pergamon Press Ltd., Oxford, 277-284.

Kuthan, M.F., 1943: *Die Ozillation der Vulkanismus und die Tektonik von Reykjanes*. University of Bratislava, Bratislava, 108 pp.

Mnzava, F.J., 2014: Subsurface geology and hydrothermal alteration of well HE-4, Hellisheidi geothermal field, SW- Iceland. Report 20 in: *Geothermal Training in Iceland 2014*. UNU-GTP, Iceland, 30.

Mostaghel, B., 1999: Processing and interpretation of geophysical well logs from well KJ-32, Krafla geothermal field, NE-Iceland. Report 8 in: Geothermal training in Iceland 1999. UNU-GTP, Iceland, 193-220.

Richter, B., Gudlaugsson, S.Th., Steingrímsson, B., Björnsson, G., Bjarnason, J.Ö. and Thórhallsson, S., 1999: Svartsengi. Hola SJ.18: Borun, rannsóknir og vinnslueiginleikar: Lokaskýrsla. OS.99117/JHD.08.

Rodas M, N.R., 1996: Borehole geology and hydrothermal alteration of well SV-14, Svartsengi, SW-Iceland. Report 15 in: *Geothermal Training in Iceland 1996*. UNU-GTP, Iceland, 22.

Saemundsson, K., 2015: *Revised map of the Svartsengi, Eldvörp and Reykjanes geological map, unpublished. Based on the Eldvörp and Reykjanes geological map (bedrock), 1:25.000.* Orkustofnun, Hitaveita Sudurnesja and Landmaelingar Íslands, 1995.

Saemundsson, K., 1979: Outline of the geology of Iceland. *Jokull 29*, 7-28.

Sigurdsson, F., 1985: *Groundwater and hydrogeology of the outer Reykjanes Peninsula*. Orkustofnun, Reykjavík, report OS-85075/VOD-06 (in Icelandic), 194 pp.

Sigurdsson, Ó. and Fridleifsson, G.Ó., 2015: *Design criteria for production well SV.26, revised.* HS Orka, HF., Memorandum 9.12.2015.

Steingrímsson, B., 2011: Geothermal well logging cement bond and caliper logs. *Papers presented at Short Course on Geothermal Drilling, Resource Development and Power Plants, organized by UNUGTP and LaGeo, Santa Tecla, El Salvador*, 11 pp.

Thórdarson, T., 2012: *Outline of geology of Iceland.* Chapman Conference, 2012.

Weisenberger, T.B., Gudjónsdóttir, S.R., Tryggvason, H., Hardarson, B.S., Gunnarsdóttir, S.H., Níelsson, S., Sigurgeirsson, M.Á., Einarsson, G.M., Kristinsson, B., Pétursson, F., Ingólfsson, H., Stefánsson, H.Ö., Jónasson, H., Tulinius, H., and Gunnarsson B.S., 2016: *Well report – SV-26. Drilling of well SV-26 in Svartsengi from surface down to 2537 m and geothermal studies during the drilling of the well.* ÍSOR – Iceland GeoSurvey, Reykjavík, report ÍSOR-2016/022, prepared for HS Orka Ltd., 143 pp.

Weisenberger, T. and Selbekk, R.S., 2009: Multi-stage zeolite facies mineralization in the Hvalfjördur area, Iceland. *International Journal of Earth Sciences, 98*, 985–999.

Worku, S., 2012: Borehole geology and hydrothermal mineral alteration of well HN-3, Hellisheidi Iceland, geothermal field, SW-Iceland. Report 37 in: *Geothermal training in Iceland 2012*. UNU-GTP, Iceland, 953-986.

APPENDIX I: Temperature and geophysical logs

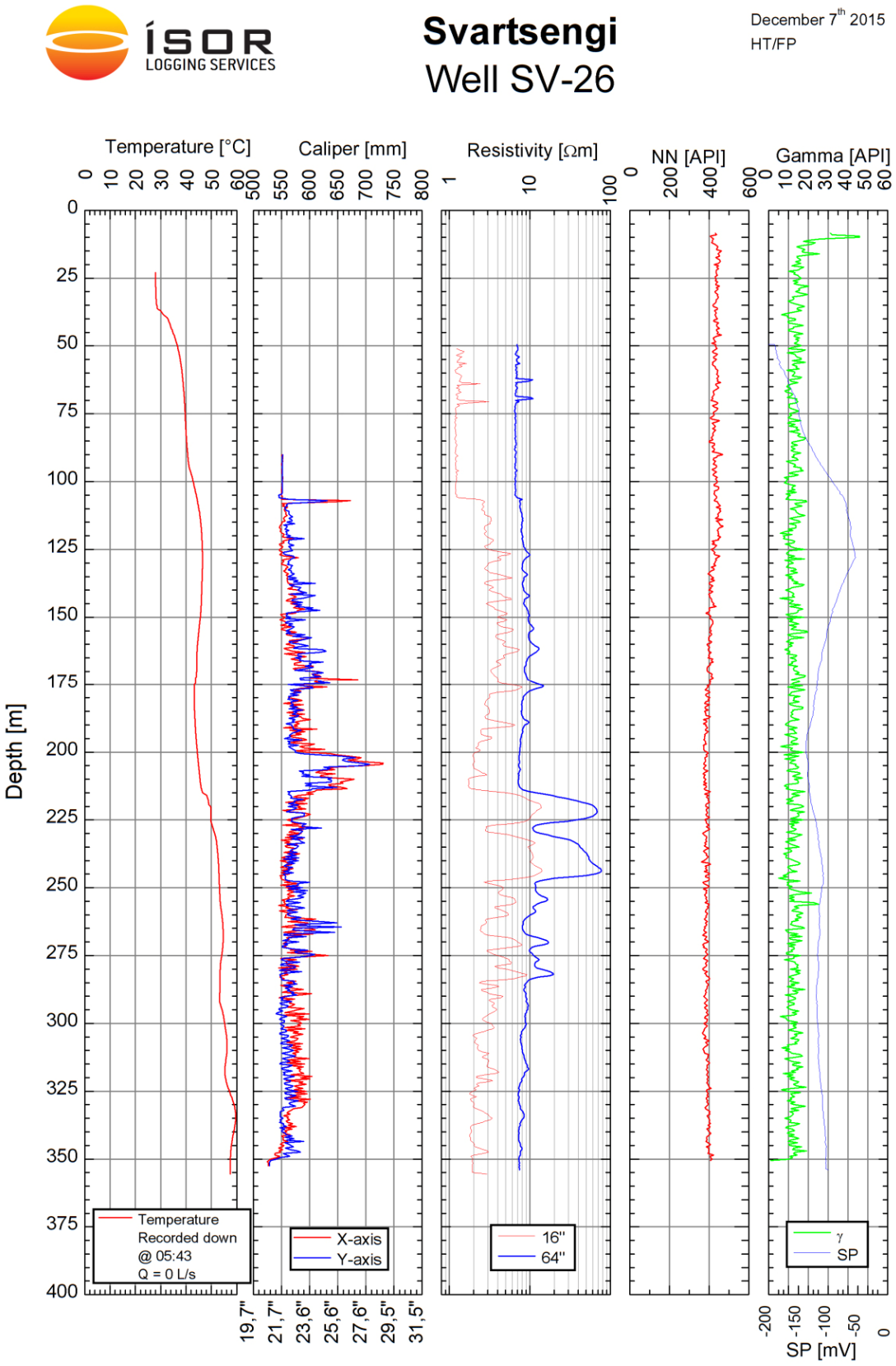

FIGURE 1: Geophysical logs after phase 1 of the drilling of well SV-26. (Weisenberger et al., 2016)

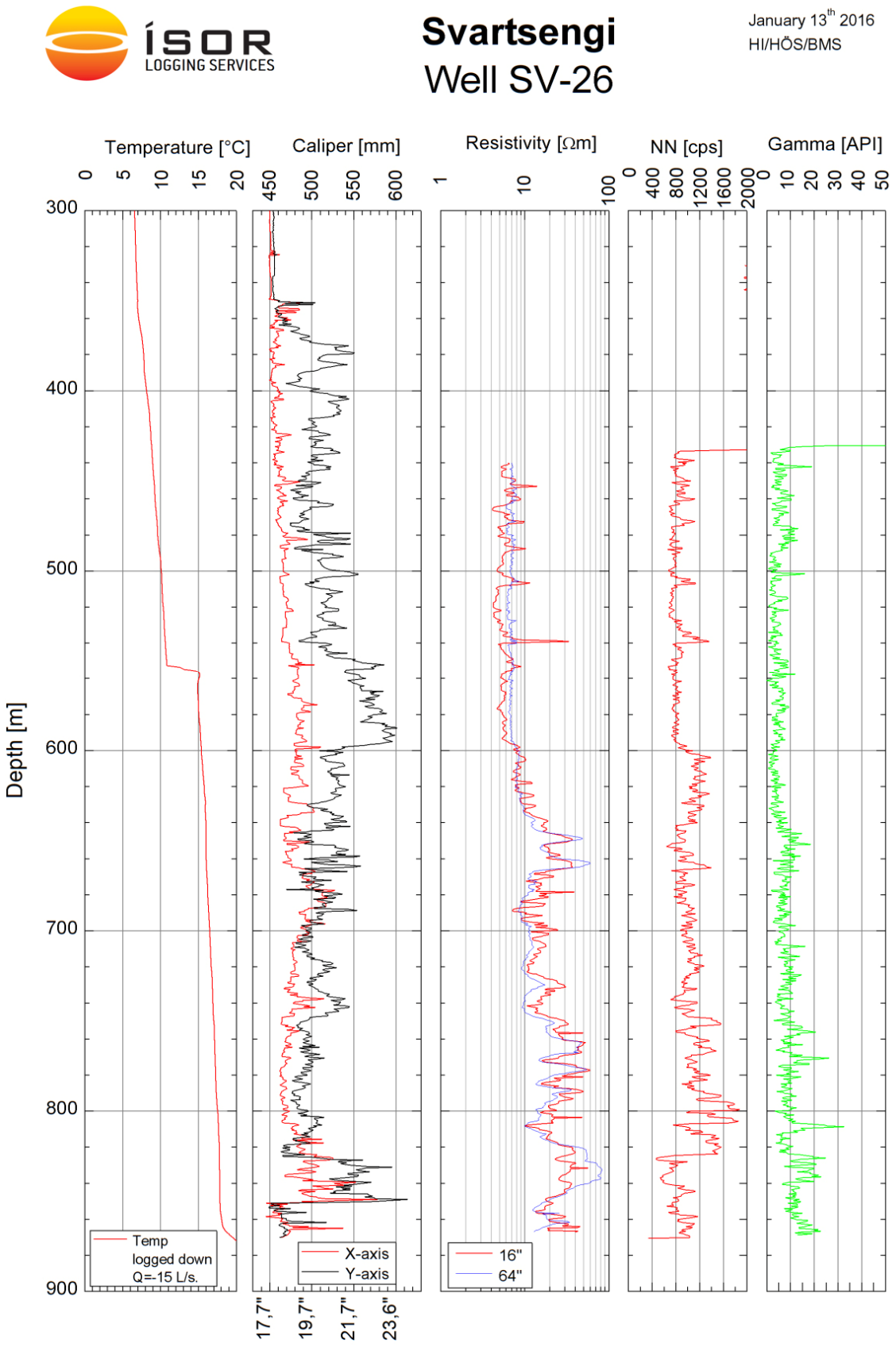

FIGURE 2: Geophysical logs after phase 2 of the drilling of well SV-26. (Weisenberger et al., 2016)

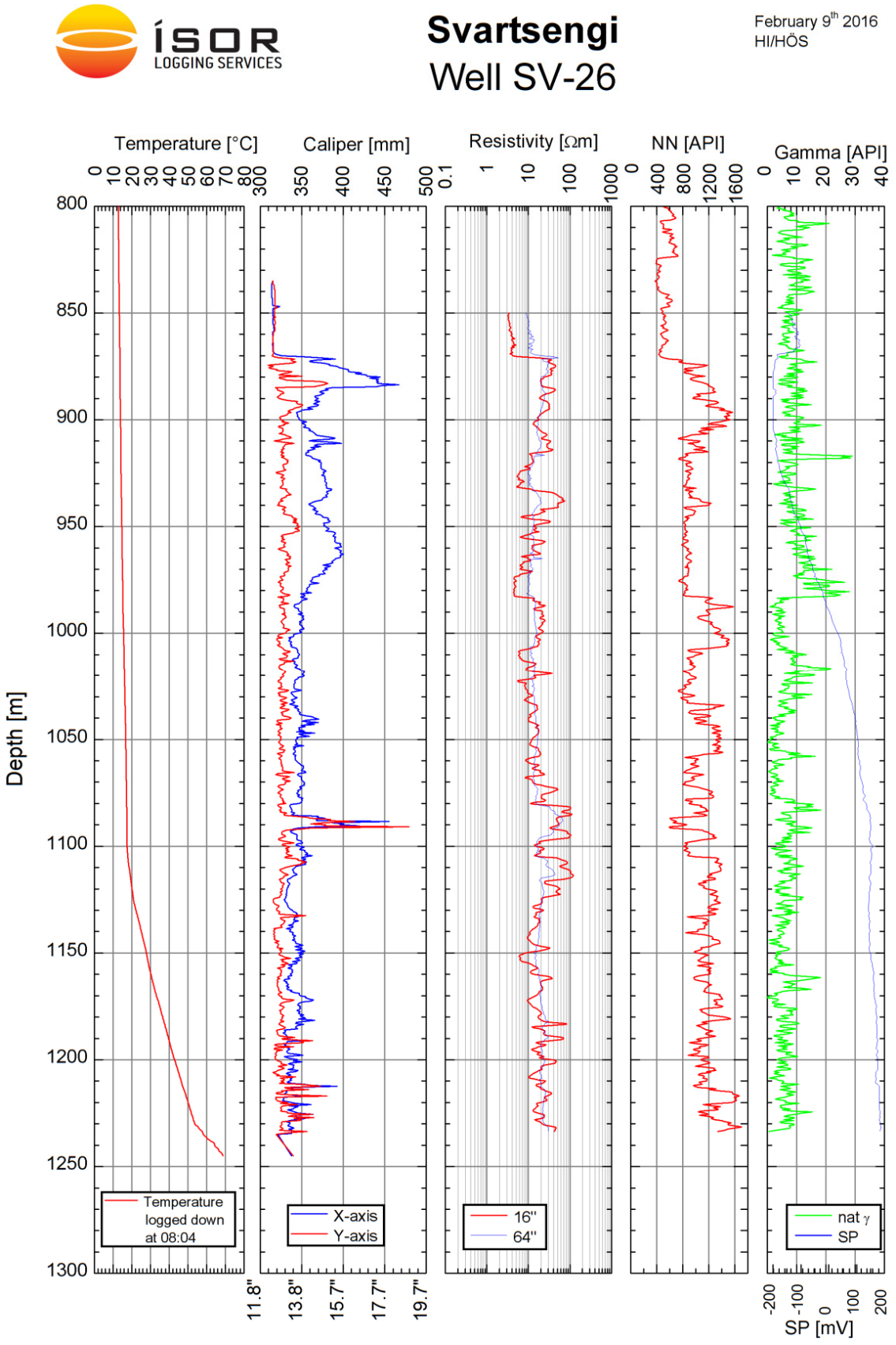

FIGURE 3: Geophysical logs after phase 3 of the drilling of well SV-26. (Weisenberger et al., 2016)

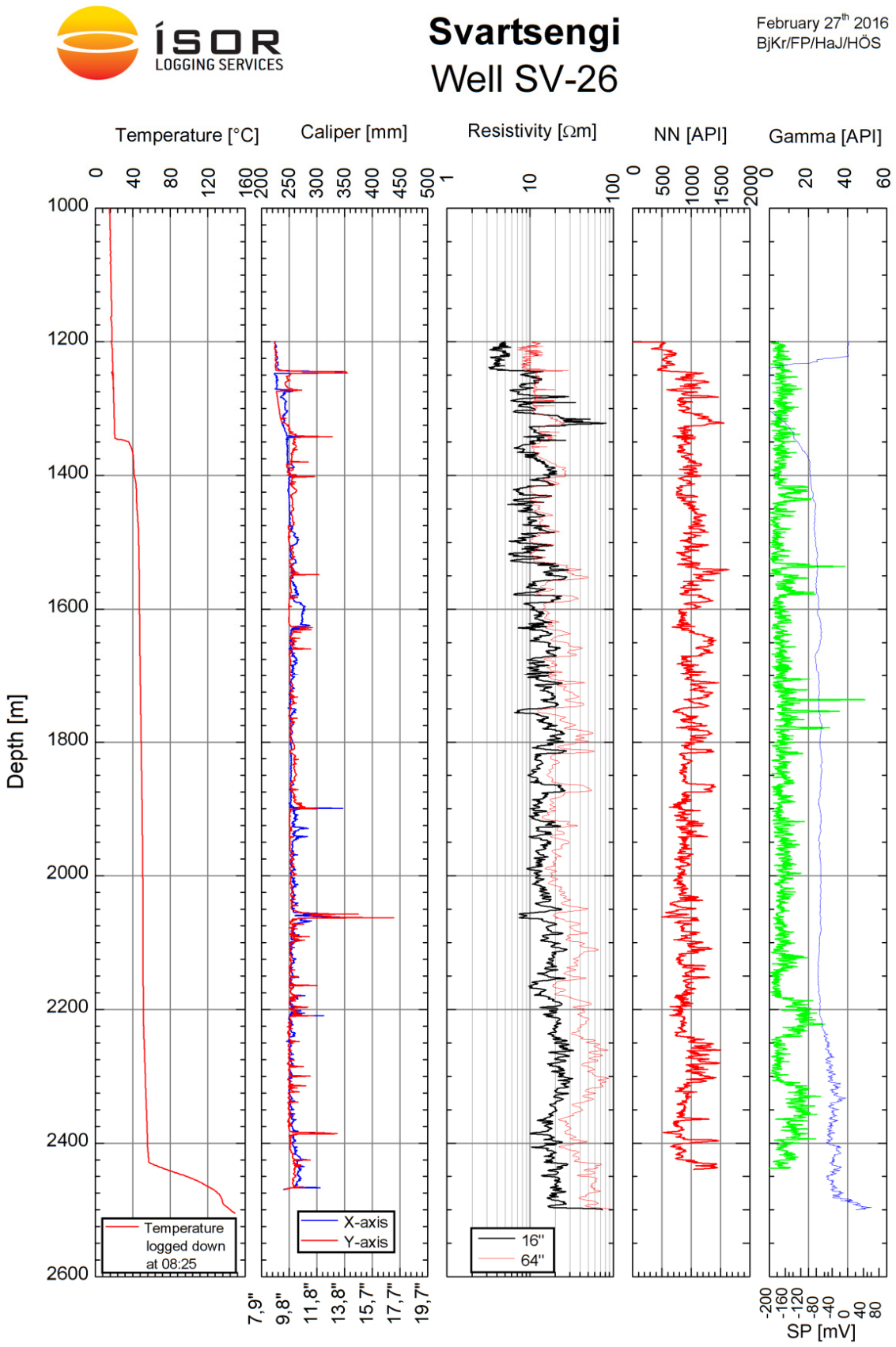

FIGURE 4: Geophysical logs after phase 4 of the drilling of well SV-26. (Weisenberger et al., 2016)

APPENDIX II: Fluid inclusion results

Depth (m) MD	Crystal	Histogram X=Temperature range (°C) Y= Number of fluid inclusions
662-666	Quartz	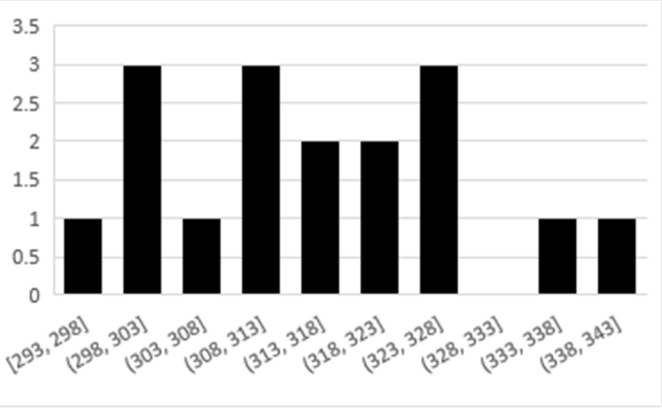
808	Quartz	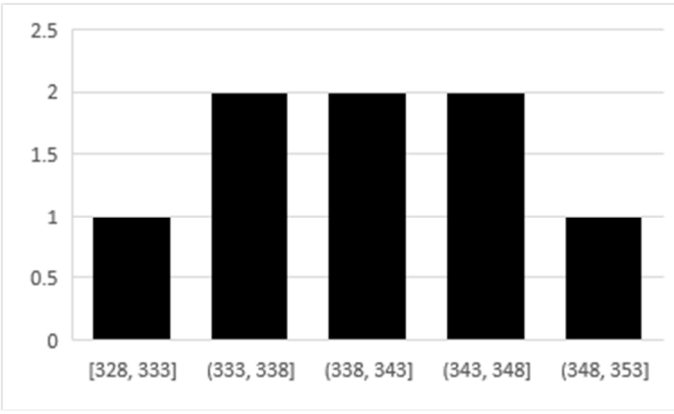
1046-1062	Quartz	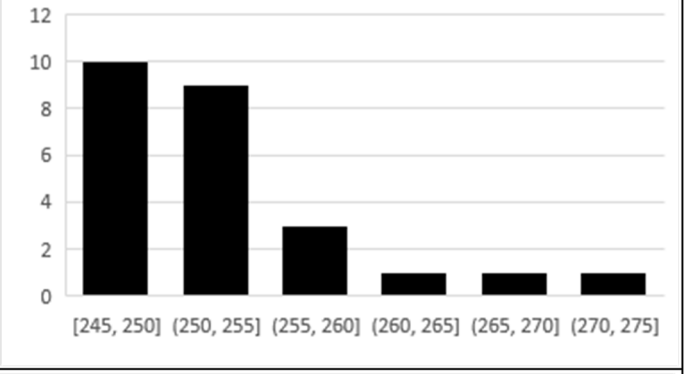
1292	Calcite	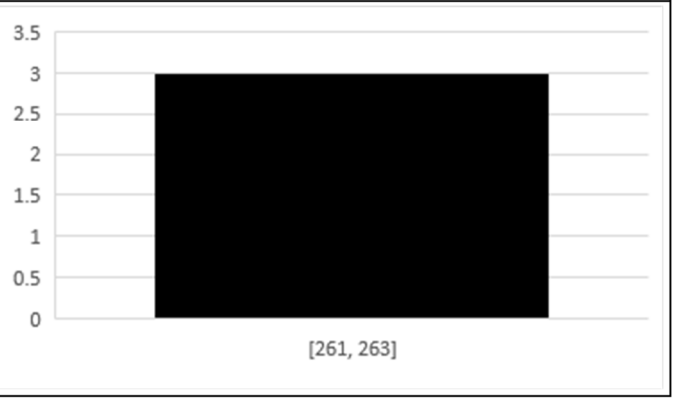

FIGURE 1: Histogram diagram showing the variations of homogenization temperatures in well SV-26

TABLE 2: Homogenization of fluid inclusion

Depth (m) MD	Sample	Mineral	Inclusion	Homonization Temperature (°C)
662	1	Quartz	1	313
	1		2	299
	1		3	308
	1		4	300
	1		5	300
	1		6	318
	1		7	293
	1		8	319
666	1	Quartz	1	325
	1		2	320
	1		3	328
	1		4	341
	1		5	336
	1		6	328
	1		7	310
	1		8	311
	1		9	310
808	1	Quartz	1	346
	1		2	351
	1		3	328
	1		4	337
	1		5	343
	1		6	335
	1		7	342
	1		8	342
1046	1	Quartz	1	245
	2		1	262
	2		2	248
	2		3	250
	2		4	257
	2		5	266
	2		6	251
	2		7	251
1062	1	Quartz	1	256
	1		2	257
	1		3	255
	1		4	255
	1		5	255
	1		6	252
	1		7	252
	1		8	251
	2	Quartz	1	272
	2		2	250
	2		3	249
	2		4	249
	2		5	249
	2		6	249
	2		7	251
	2		8	250
	2		9	250
1292	1	Calcite	1	261
	1		2	262
	1		3	263

APPENDIX III: XRD results

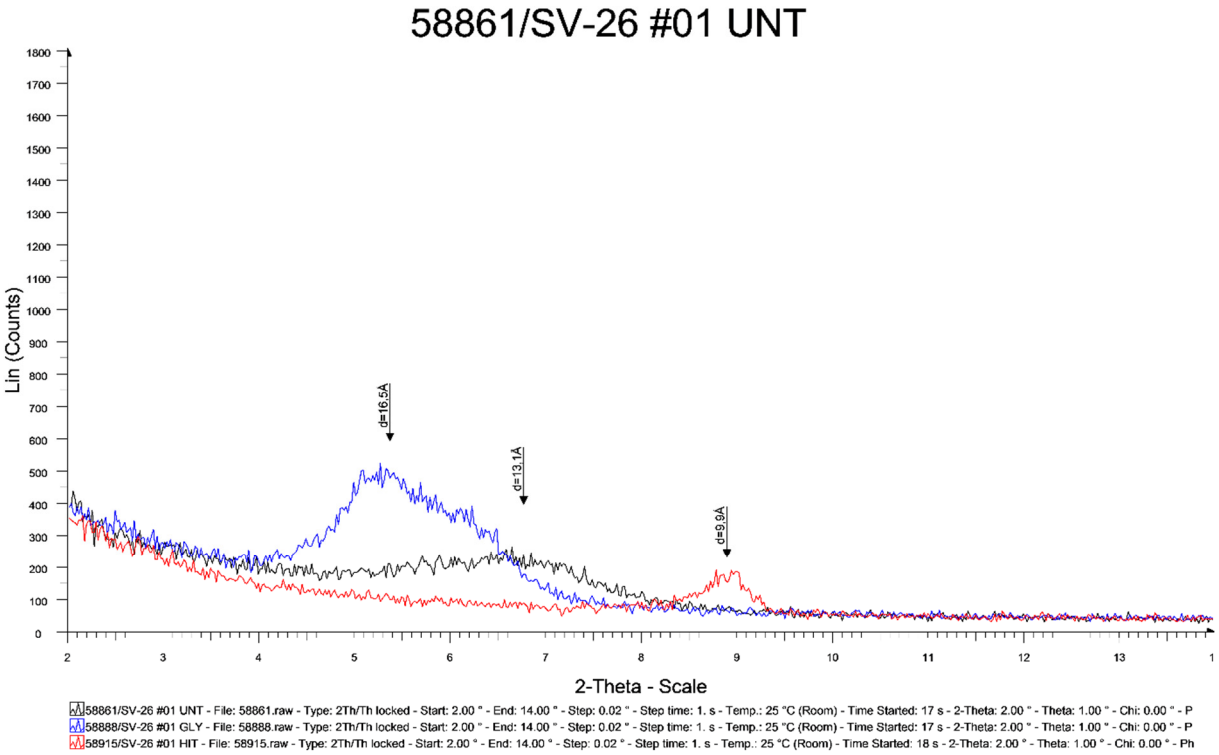

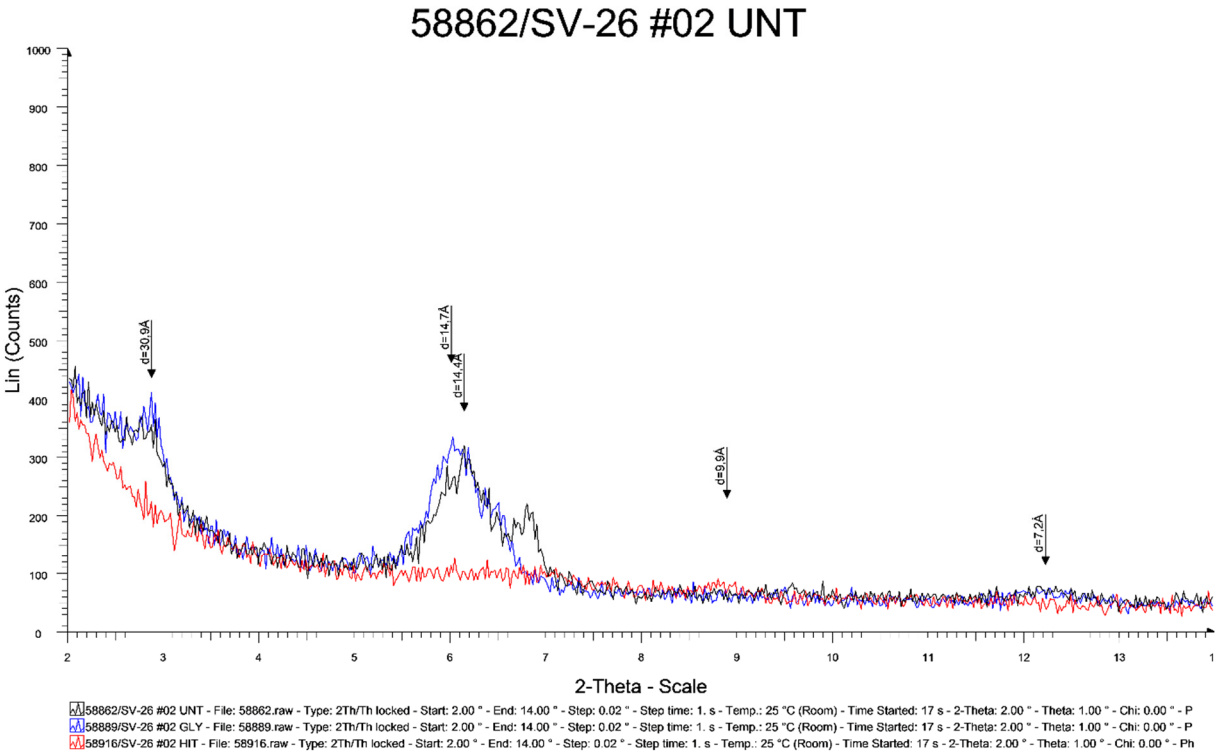

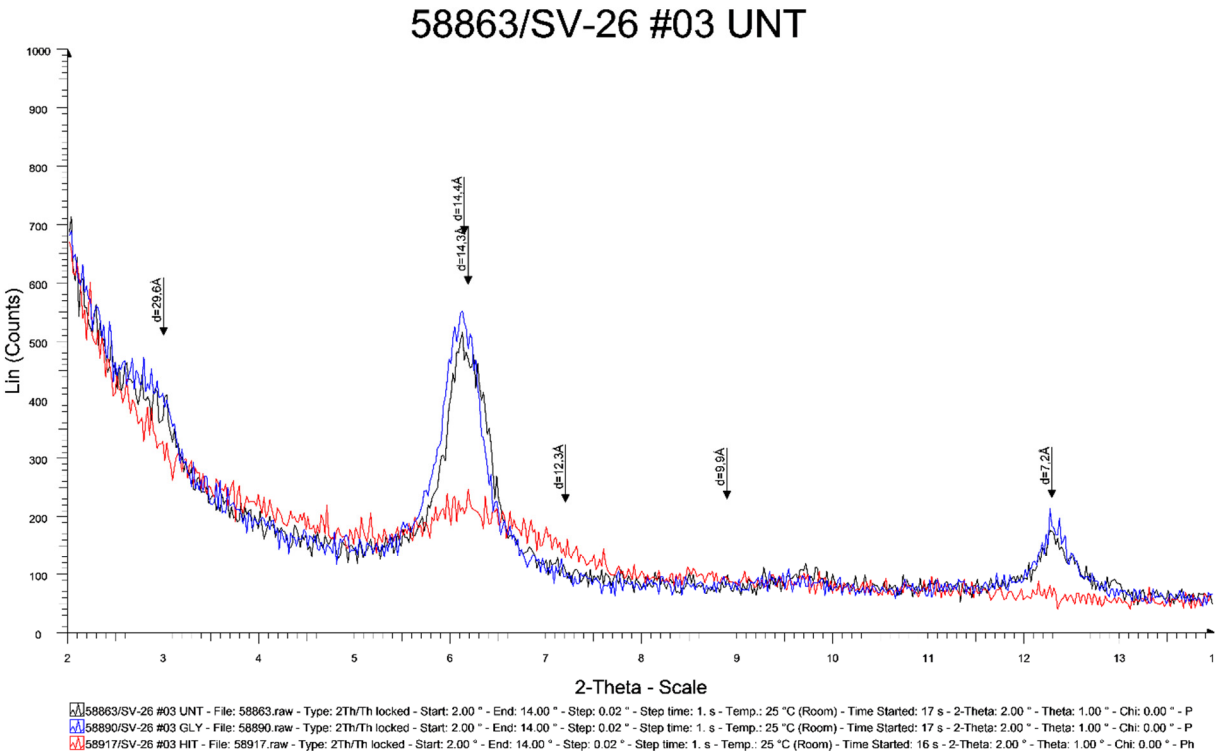
58863/SV-26 #03 UNT
Lin (Counts)
2-Theta - Scale
d=29.6Å
d=14.3Å
d=14.4Å
d=12.3Å
d=9.9Å
d=7.2Å
58863/SV-26 #03 UNT - File: 58863.raw - Type: 2Th/Th locked - Start: 2.00 ° - End: 14.00 ° - Step: 0.02 ° - Step time: 1. s - Temp.: 25 °C (Room) - Time Started: 17 s - 2-Theta: 2.00 ° - Theta: 1.00 ° - Chi: 0.00 ° - P
58890/SV-26 #03 GLY - File: 58890.raw - Type: 2Th/Th locked - Start: 2.00 ° - End: 14.00 ° - Step: 0.02 ° - Step time: 1. s - Temp.: 25 °C (Room) - Time Started: 17 s - 2-Theta: 2.00 ° - Theta: 1.00 ° - Chi: 0.00 ° - P
58917/SV-26 #03 HIT - File: 58917.raw - Type: 2Th/Th locked - Start: 2.00 ° - End: 14.00 ° - Step: 0.02 ° - Step time: 1. s - Temp.: 25 °C (Room) - Time Started: 16 s - 2-Theta: 2.00 ° - Theta: 1.00 ° - Chi: 0.00 ° - Ph

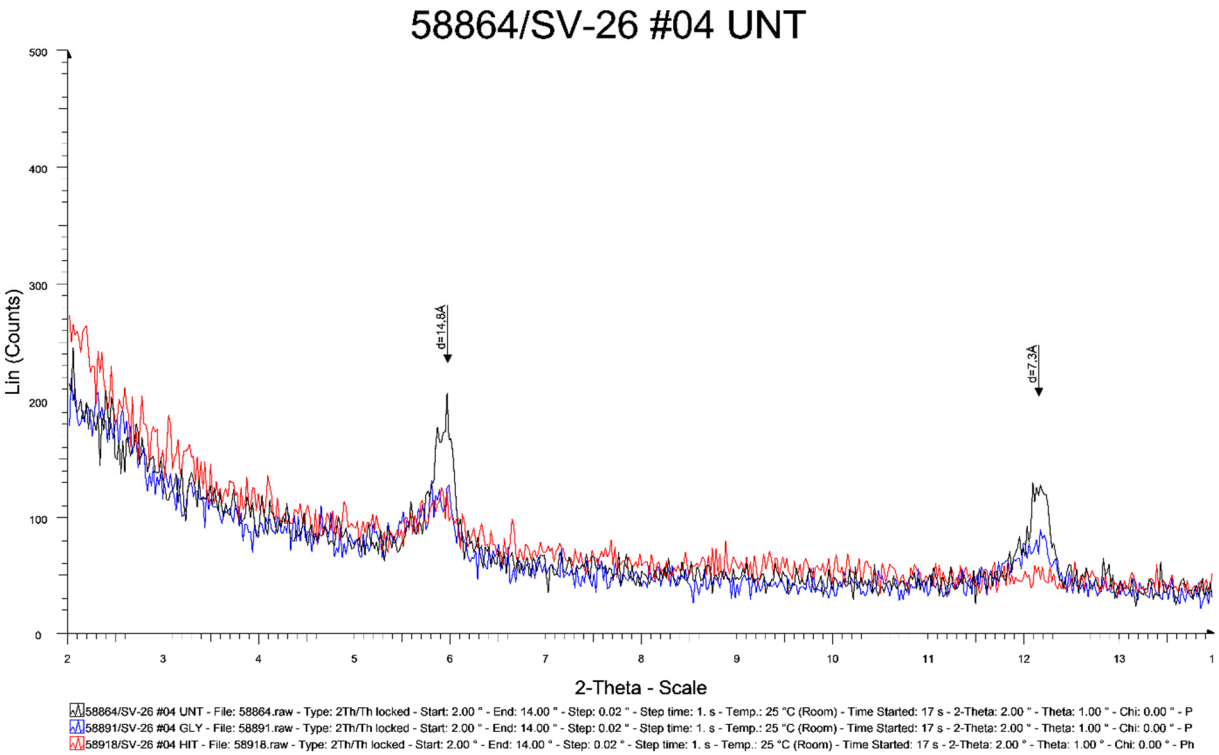
58864/SV-26 #04 UNT
Lin (Counts)
2-Theta - Scale
d=14.8Å
d=7.3Å
58864/SV-26 #04 UNT - File: 58864.raw - Type: 2Th/Th locked - Start: 2.00 ° - End: 14.00 ° - Step: 0.02 ° - Step time: 1. s - Temp.: 25 °C (Room) - Time Started: 17 s - 2-Theta: 2.00 ° - Theta: 1.00 ° - Chi: 0.00 ° - P
58891/SV-26 #04 GLY - File: 58891.raw - Type: 2Th/Th locked - Start: 2.00 ° - End: 14.00 ° - Step: 0.02 ° - Step time: 1. s - Temp.: 25 °C (Room) - Time Started: 17 s - 2-Theta: 2.00 ° - Theta: 1.00 ° - Chi: 0.00 ° - P
58918/SV-26 #04 HIT - File: 58918.raw - Type: 2Th/Th locked - Start: 2.00 ° - End: 14.00 ° - Step: 0.02 ° - Step time: 1. s - Temp.: 25 °C (Room) - Time Started: 17 s - 2-Theta: 2.00 ° - Theta: 1.00 ° - Chi: 0.00 ° - Ph

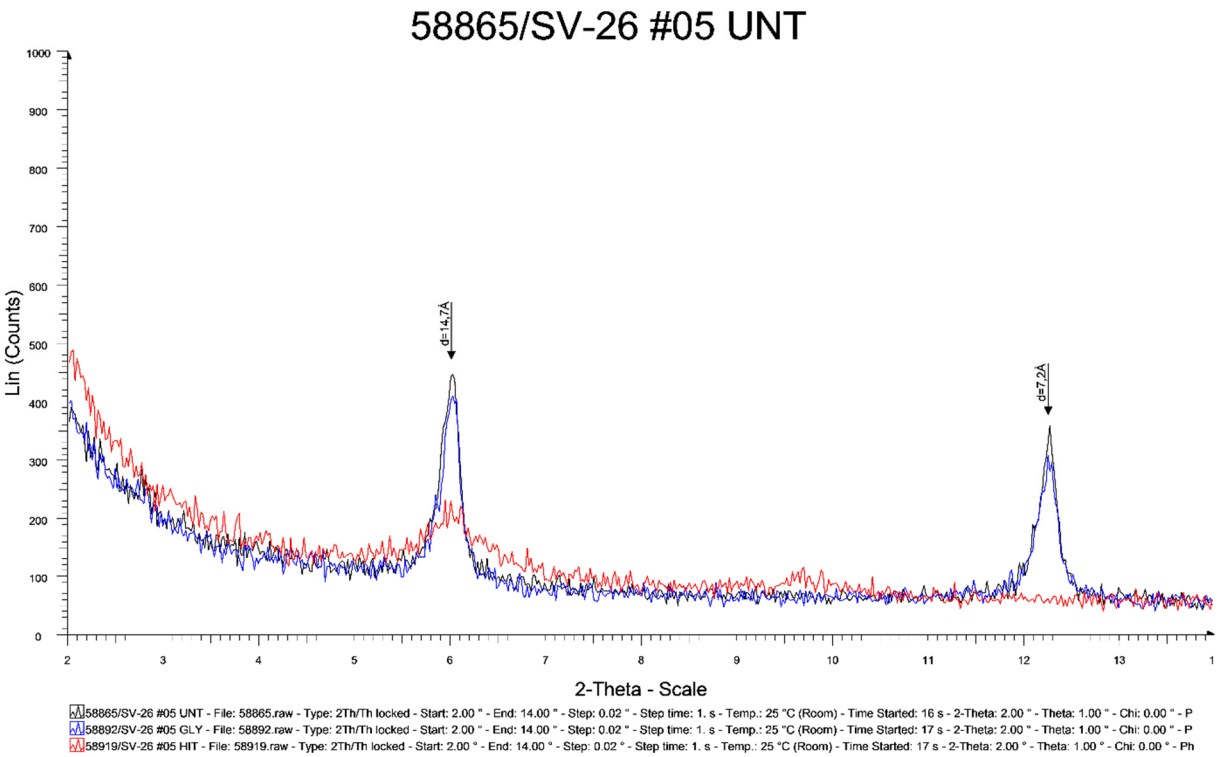
58865/SV-26 #05 UNT
Lin (Counts)
2-Theta - Scale
d=14.7Å
d=7.2Å
58865/SV-26 #05 UNT - File: 58865.raw - Type: 2Th/Th locked - Start: 2.00 ° - End: 14.00 ° - Step: 0.02 ° - Step time: 1. s - Temp.: 25 °C (Room) - Time Started: 16 s - 2-Theta: 2.00 ° - Theta: 1.00 ° - Chi: 0.00 ° - P
58892/SV-26 #05 GLY - File: 58892.raw - Type: 2Th/Th locked - Start: 2.00 ° - End: 14.00 ° - Step: 0.02 ° - Step time: 1. s - Temp.: 25 °C (Room) - Time Started: 17 s - 2-Theta: 2.00 ° - Theta: 1.00 ° - Chi: 0.00 ° - P
58919/SV-26 #05 HIT - File: 58919.raw - Type: 2Th/Th locked - Start: 2.00 ° - End: 14.00 ° - Step: 0.02 ° - Step time: 1. s - Temp.: 25 °C (Room) - Time Started: 17 s - 2-Theta: 2.00 ° - Theta: 1.00 ° - Chi: 0.00 ° - Ph

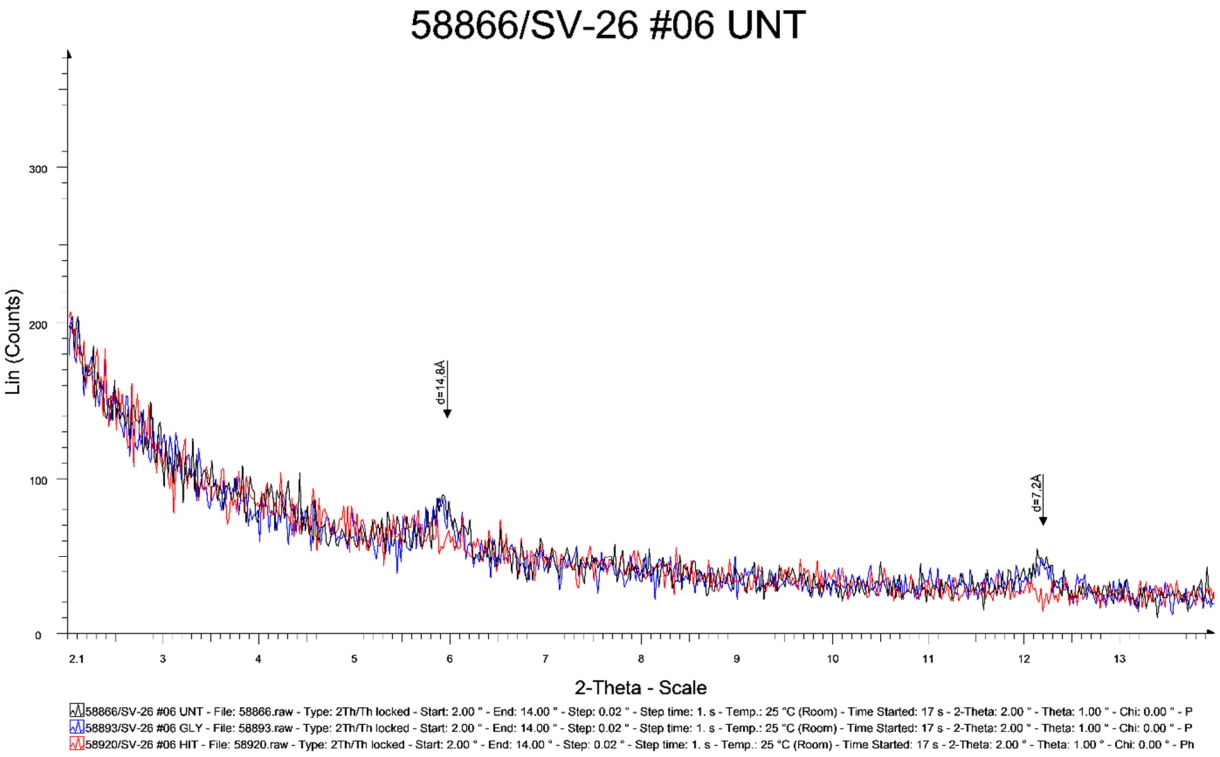
58866/SV-26 #06 UNT
Lin (Counts)
2-Theta - Scale
d=14.6Å
d=7.2Å
58866/SV-26 #06 UNT - File: 58866.raw - Type: 2Th/Th locked - Start: 2.00 ° - End: 14.00 ° - Step: 0.02 ° - Step time: 1. s - Temp.: 25 °C (Room) - Time Started: 17 s - 2-Theta: 2.00 ° - Theta: 1.00 ° - Chi: 0.00 ° - P
58893/SV-26 #06 GLY - File: 58893.raw - Type: 2Th/Th locked - Start: 2.00 ° - End: 14.00 ° - Step: 0.02 ° - Step time: 1. s - Temp.: 25 °C (Room) - Time Started: 17 s - 2-Theta: 2.00 ° - Theta: 1.00 ° - Chi: 0.00 ° - P
58920/SV-26 #06 HIT - File: 58920.raw - Type: 2Th/Th locked - Start: 2.00 ° - End: 14.00 ° - Step: 0.02 ° - Step time: 1. s - Temp.: 25 °C (Room) - Time Started: 17 s - 2-Theta: 2.00 ° - Theta: 1.00 ° - Chi: 0.00 ° - Ph

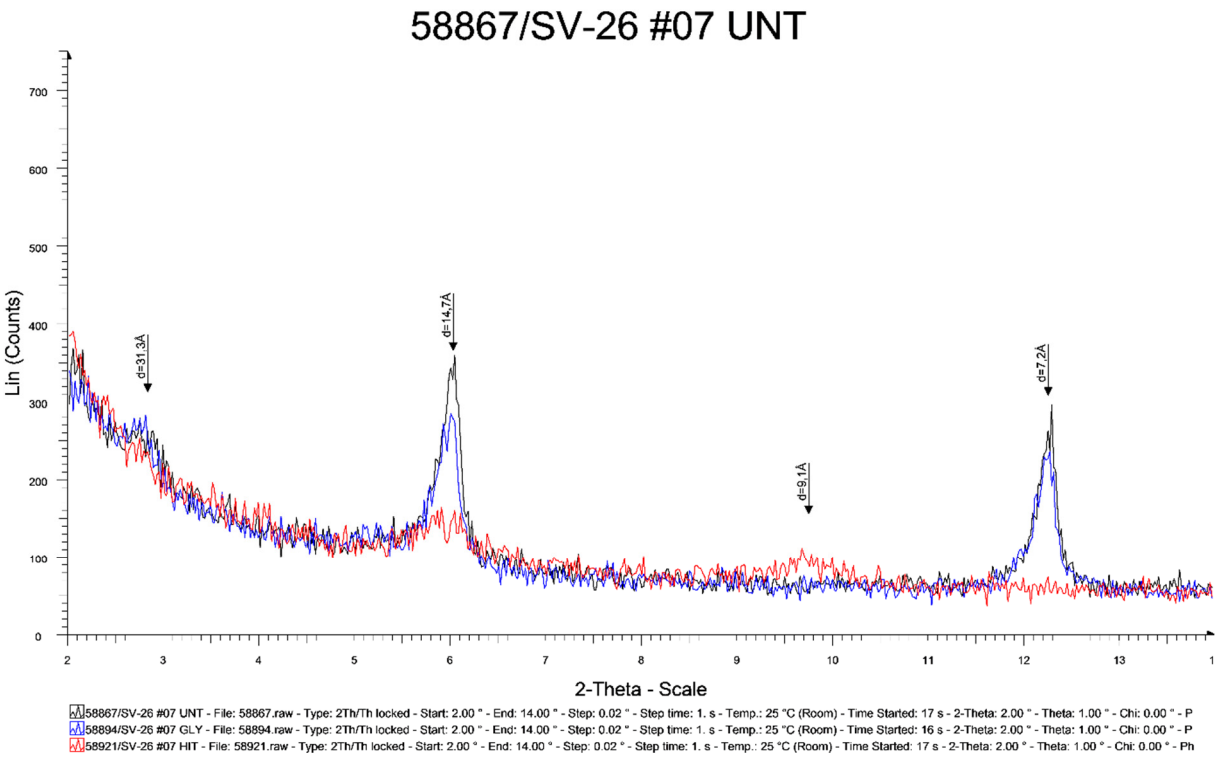
58867/SV-26 #07 UNT
Lin (Counts)
2-Theta - Scale
d=31.3Å
d=14.7Å
d=9.1Å
d=7.2Å
58867/SV-26 #07 UNT - File: 58867.raw - Type: 2Th/Th locked - Start: 2.00 ° - End: 14.00 ° - Step: 0.02 ° - Step time: 1. s - Temp.: 25 °C (Room) - Time Started: 17 s - 2-Theta: 2.00 ° - Theta: 1.00 ° - Chi: 0.00 ° - P
58894/SV-26 #07 GLY - File: 58894.raw - Type: 2Th/Th locked - Start: 2.00 ° - End: 14.00 ° - Step: 0.02 ° - Step time: 1. s - Temp.: 25 °C (Room) - Time Started: 16 s - 2-Theta: 2.00 ° - Theta: 1.00 ° - Chi: 0.00 ° - P
58921/SV-26 #07 HIT - File: 58921.raw - Type: 2Th/Th locked - Start: 2.00 ° - End: 14.00 ° - Step: 0.02 ° - Step time: 1. s - Temp.: 25 °C (Room) - Time Started: 17 s - 2-Theta: 2.00 ° - Theta: 1.00 ° - Chi: 0.00 ° - Ph

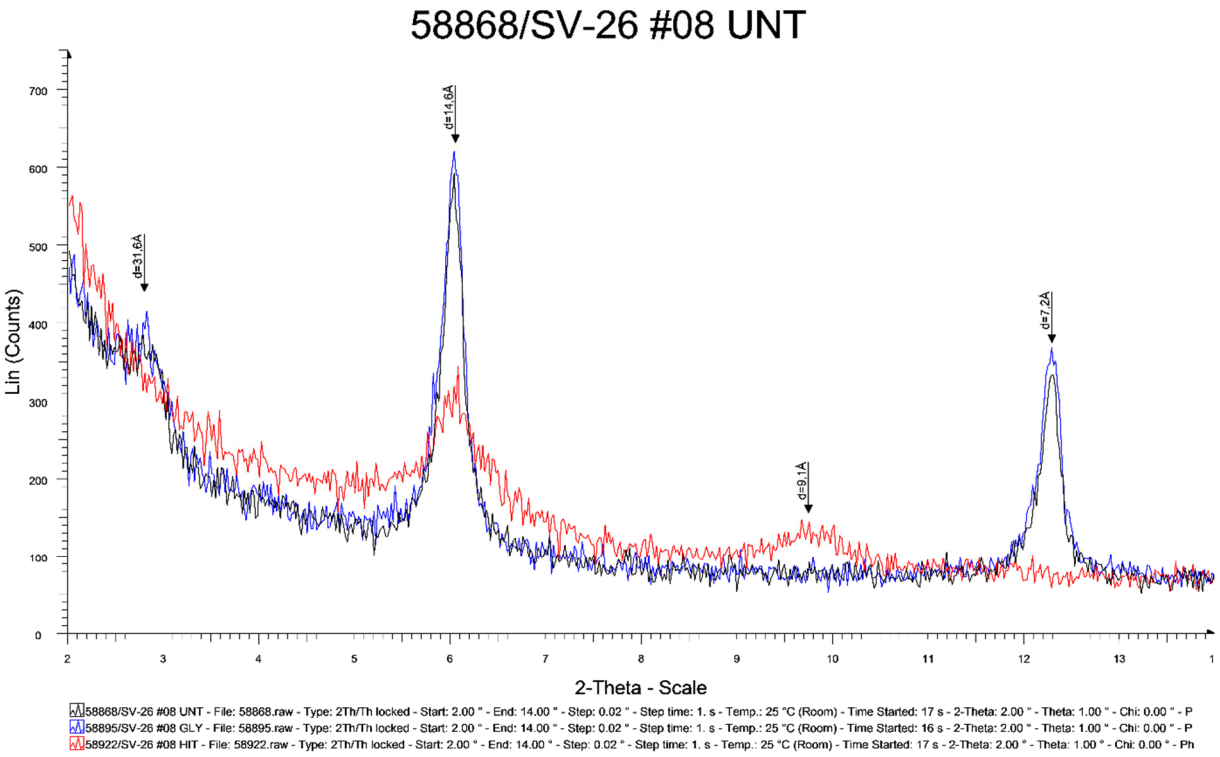
58868/SV-26 #08 UNT
Lin (Counts)
2-Theta - Scale
d=31.6Å
d=14.6Å
d=9.1Å
d=7.2Å
58868/SV-26 #08 UNT - File: 58868.raw - Type: 2Th/Th locked - Start: 2.00 ° - End: 14.00 ° - Step: 0.02 ° - Step time: 1. s - Temp.: 25 °C (Room) - Time Started: 17 s - 2-Theta: 2.00 ° - Theta: 1.00 ° - Chi: 0.00 ° - P
58895/SV-26 #08 GLY - File: 58895.raw - Type: 2Th/Th locked - Start: 2.00 ° - End: 14.00 ° - Step: 0.02 ° - Step time: 1. s - Temp.: 25 °C (Room) - Time Started: 16 s - 2-Theta: 2.00 ° - Theta: 1.00 ° - Chi: 0.00 ° - P
58922/SV-26 #08 HIT - File: 58922.raw - Type: 2Th/Th locked - Start: 2.00 ° - End: 14.00 ° - Step: 0.02 ° - Step time: 1. s - Temp.: 25 °C (Room) - Time Started: 17 s - 2-Theta: 2.00 ° - Theta: 1.00 ° - Chi: 0.00 ° - Ph

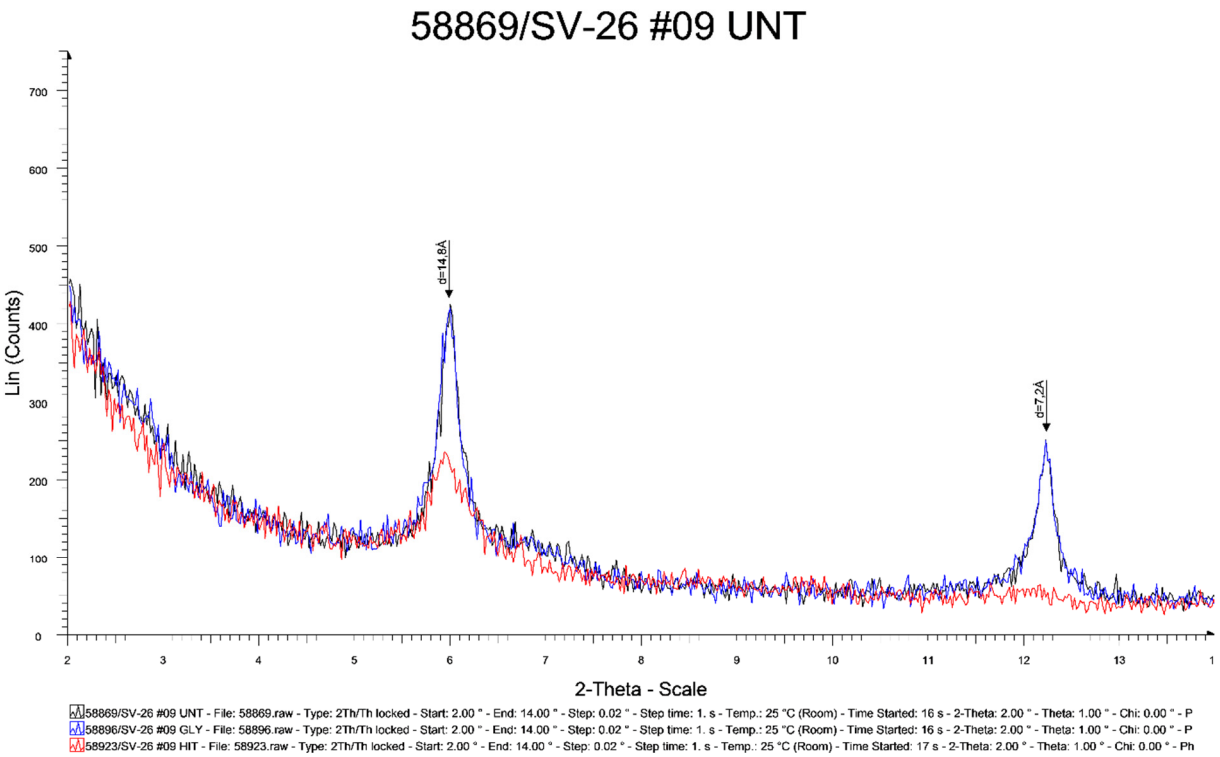
58869/SV-26 #09 UNT
Lin (Counts)
2-Theta - Scale
d=14.8Å
d=7.2Å
58869/SV-26 #09 UNT - File: 58869.raw - Type: 2Th/Th locked - Start: 2.00 ° - End: 14.00 ° - Step: 0.02 ° - Step time: 1. s - Temp.: 25 °C (Room) - Time Started: 16 s - 2-Theta: 2.00 ° - Theta: 1.00 ° - Chi: 0.00 ° - P
58896/SV-26 #09 GLY - File: 58896.raw - Type: 2Th/Th locked - Start: 2.00 ° - End: 14.00 ° - Step: 0.02 ° - Step time: 1. s - Temp.: 25 °C (Room) - Time Started: 16 s - 2-Theta: 2.00 ° - Theta: 1.00 ° - Chi: 0.00 ° - P
58923/SV-26 #09 HIT - File: 58923.raw - Type: 2Th/Th locked - Start: 2.00 ° - End: 14.00 ° - Step: 0.02 ° - Step time: 1. s - Temp.: 25 °C (Room) - Time Started: 17 s - 2-Theta: 2.00 ° - Theta: 1.00 ° - Chi: 0.00 ° - Ph

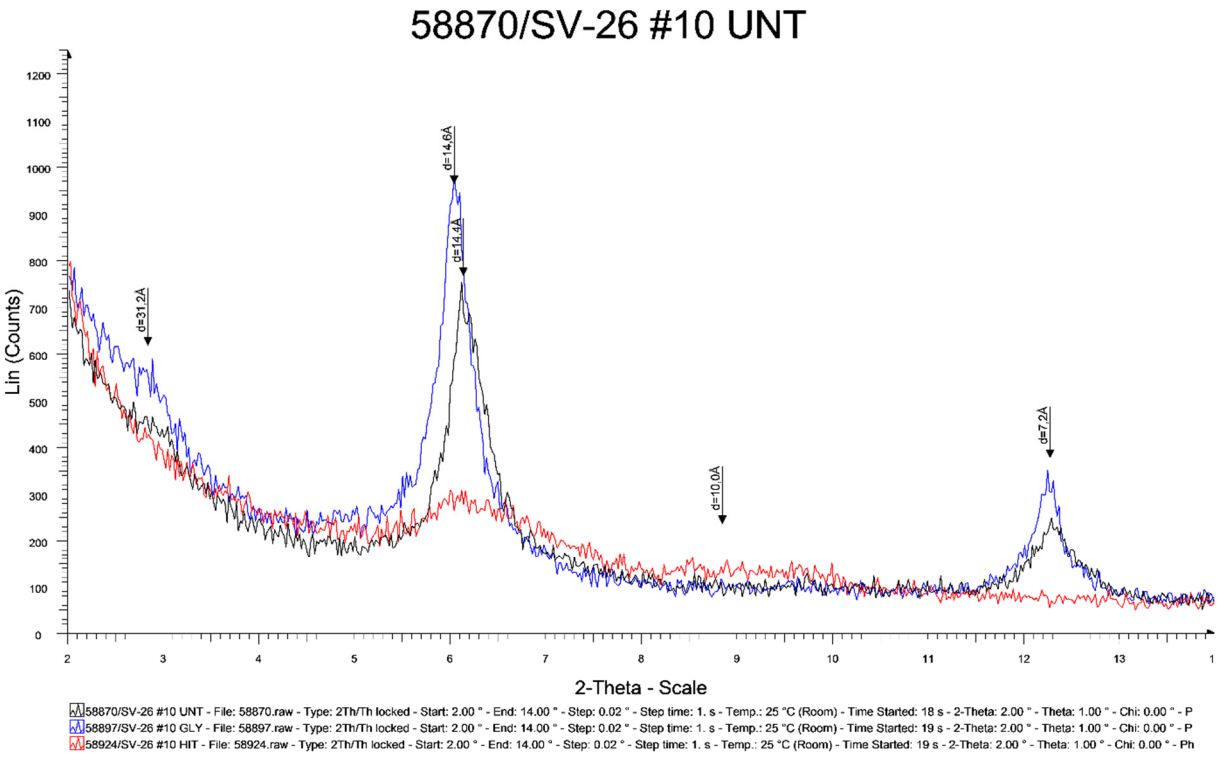
58870/SV-26 #10 UNT
Lin (Counts)
2-Theta - Scale
d=14.6Å
d=14.4Å
d=31.2Å
d=10.0Å
d=7.2Å
58870/SV-26 #10 UNT - File: 58870.raw - Type: 2Th/Th locked - Start: 2.00 ° - End: 14.00 ° - Step: 0.02 ° - Step time: 1. s - Temp.: 25 °C (Room) - Time Started: 18 s - 2-Theta: 2.00 ° - Theta: 1.00 ° - Chi: 0.00 ° - P
58897/SV-26 #10 GLY - File: 58897.raw - Type: 2Th/Th locked - Start: 2.00 ° - End: 14.00 ° - Step: 0.02 ° - Step time: 1. s - Temp.: 25 °C (Room) - Time Started: 19 s - 2-Theta: 2.00 ° - Theta: 1.00 ° - Chi: 0.00 ° - P
58924/SV-26 #10 HIT - File: 58924.raw - Type: 2Th/Th locked - Start: 2.00 ° - End: 14.00 ° - Step: 0.02 ° - Step time: 1. s - Temp.: 25 °C (Room) - Time Started: 19 s - 2-Theta: 2.00 ° - Theta: 1.00 ° - Chi: 0.00 ° - Ph

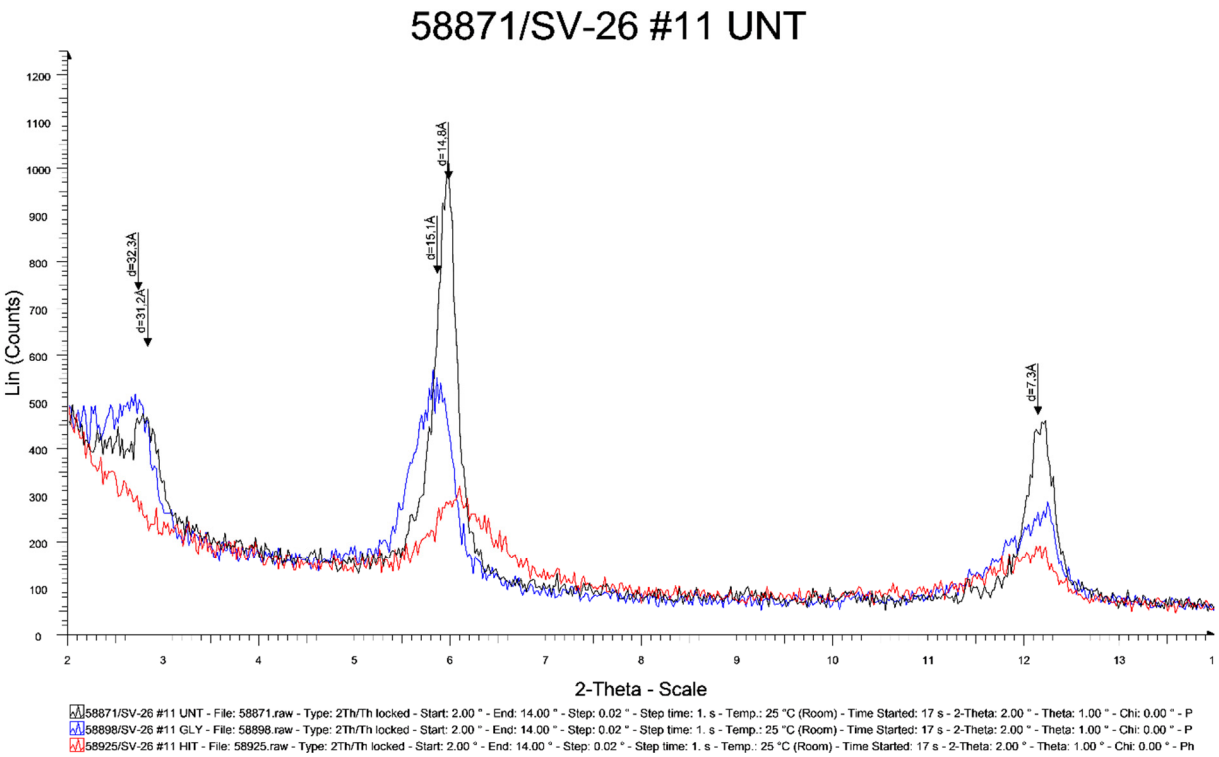
58871/SV-26 #11 UNT
Lin (Counts)
2-Theta - Scale
d=32.3Å
d=31.2Å
d=15.1Å
d=14.8Å
d=7.3Å
58871/SV-26 #11 UNT - File: 58871.raw - Type: 2Th/Th locked - Start: 2.00 ° - End: 14.00 ° - Step: 0.02 ° - Step time: 1. s - Temp.: 25 °C (Room) - Time Started: 17 s - 2-Theta: 2.00 ° - Theta: 1.00 ° - Chi: 0.00 ° - P
58898/SV-26 #11 GLY - File: 58898.raw - Type: 2Th/Th locked - Start: 2.00 ° - End: 14.00 ° - Step: 0.02 ° - Step time: 1. s - Temp.: 25 °C (Room) - Time Started: 17 s - 2-Theta: 2.00 ° - Theta: 1.00 ° - Chi: 0.00 ° - P
58925/SV-26 #11 HIT - File: 58925.raw - Type: 2Th/Th locked - Start: 2.00 ° - End: 14.00 ° - Step: 0.02 ° - Step time: 1. s - Temp.: 25 °C (Room) - Time Started: 17 s - 2-Theta: 2.00 ° - Theta: 1.00 ° - Chi: 0.00 ° - Ph

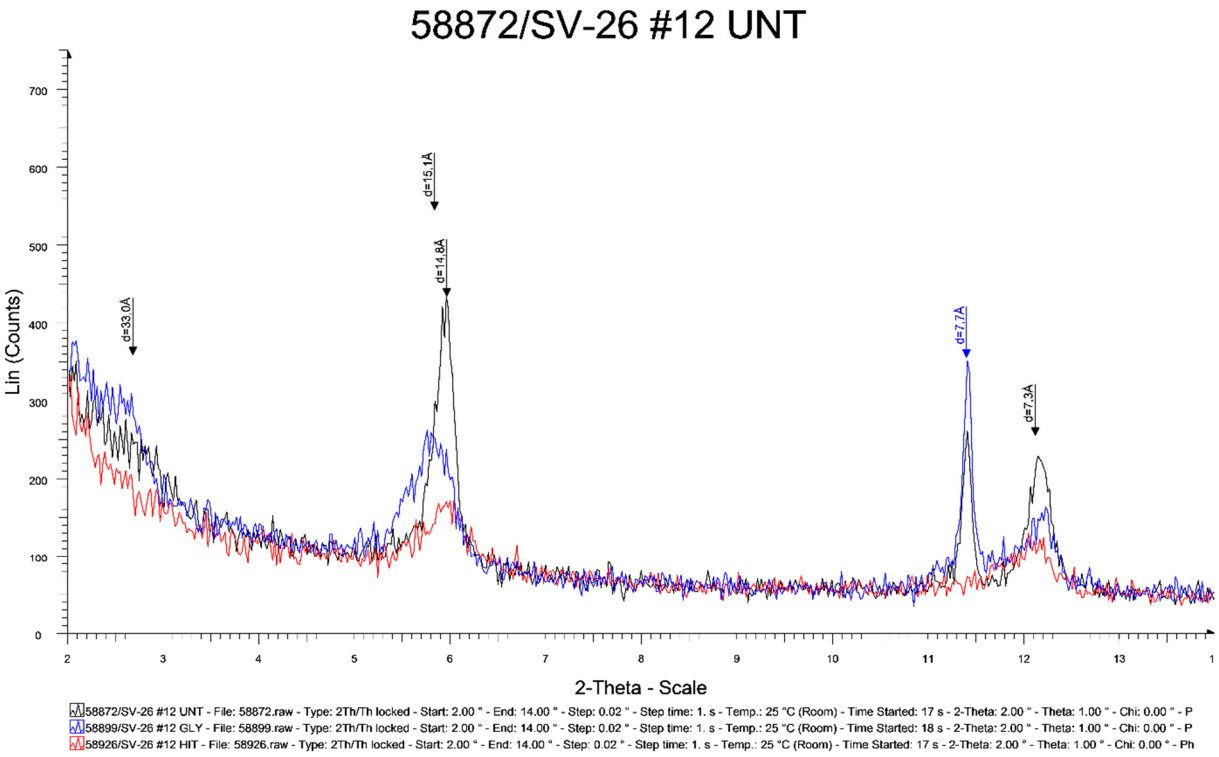
58872/SV-26 #12 UNT
Lin (Counts)
2-Theta - Scale
d=33.0Å
d=15.1Å
d=14.8Å
d=7.7Å
d=7.3Å
58872/SV-26 #12 UNT - File: 58872.raw - Type: 2Th/Th locked - Start: 2.00 ° - End: 14.00 ° - Step: 0.02 ° - Step time: 1. s - Temp.: 25 °C (Room) - Time Started: 17 s - 2-Theta: 2.00 ° - Theta: 1.00 ° - Chi: 0.00 ° - P
58899/SV-26 #12 GLY - File: 58899.raw - Type: 2Th/Th locked - Start: 2.00 ° - End: 14.00 ° - Step: 0.02 ° - Step time: 1. s - Temp.: 25 °C (Room) - Time Started: 18 s - 2-Theta: 2.00 ° - Theta: 1.00 ° - Chi: 0.00 ° - P
58926/SV-26 #12 HIT - File: 58926.raw - Type: 2Th/Th locked - Start: 2.00 ° - End: 14.00 ° - Step: 0.02 ° - Step time: 1. s - Temp.: 25 °C (Room) - Time Started: 17 s - 2-Theta: 2.00 ° - Theta: 1.00 ° - Chi: 0.00 ° - Ph

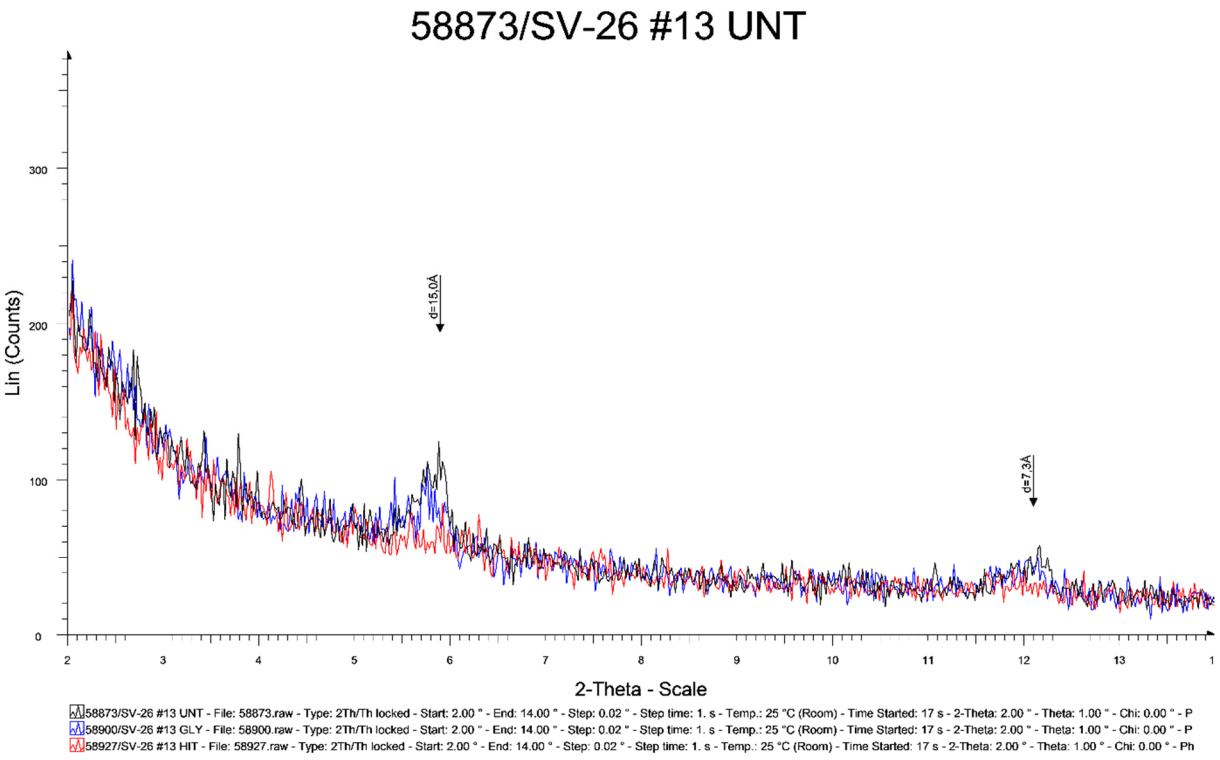
58873/SV-26 #13 UNT
Lin (Counts)
300
200
100
0
d=15.0Å
d=7.3Å
2
3
4
5
6
7
8
9
10
11
12
13
2-Theta - Scale
58873/SV-26 #13 UNT - File: 58873.raw - Type: 2Th/Th locked - Start: 2.00 ° - End: 14.00 ° - Step: 0.02 ° - Step time: 1. s - Temp.: 25 °C (Room) - Time Started: 17 s - 2-Theta: 2.00 ° - Theta: 1.00 ° - Chi: 0.00 ° - P
58900/SV-26 #13 GLY - File: 58900.raw - Type: 2Th/Th locked - Start: 2.00 ° - End: 14.00 ° - Step: 0.02 ° - Step time: 1. s - Temp.: 25 °C (Room) - Time Started: 17 s - 2-Theta: 2.00 ° - Theta: 1.00 ° - Chi: 0.00 ° - P
58927/SV-26 #13 HIT - File: 58927.raw - Type: 2Th/Th locked - Start: 2.00 ° - End: 14.00 ° - Step: 0.02 ° - Step time: 1. s - Temp.: 25 °C (Room) - Time Started: 17 s - 2-Theta: 2.00 ° - Theta: 1.00 ° - Chi: 0.00 ° - Ph